JBC RESEARCH ARTICLE

Biophysical analysis of the plant-specific GIPC sphingolipids reveals multiple modes of membrane regulation

Received for publication, November 25, 2020, and in revised form, March 3, 2021 Published, Papers in Press, March 27, 2021,
https://doi.org/10.1016/j.jbc.2021.100602

Adiilah Mamode Cassim[1], Yotam Navon[2], Yu Gao[3,4], Marion Decossas[5], Laetitia Fouillen[1], Axelle Grélard[5], Minoru Nagano[1,6], Olivier Lambert[5], Delphine Bahammou[1], Pierre Van Delft[1], Lilly Maneta-Peyret[1], Françoise Simon-Plas[7], Laurent Heux[2], Bruno Jean[2], Giovanna Fragneto[8], Jenny C. Mortimer[3,4], Magali Deleu[9], Laurence Lins[9], and Sébastien Mongrand[1,*]

From the [1]Laboratoire de Biogènese Membranaire, UMR 5200, CNRS, Université de Bordeaux, Villenave d'Ornon Cedex, France; [2]Centre de Recherches sur les Macromolécules Végétales (CERMAV), Univ. Grenoble Alpes, CNRS, Grenoble, France; [3]Joint BioEnergy Institute, Emeryville, California, USA; [4]Environmental and Systems Genomics, Lawrence Berkeley National Laboratory, Berkeley, California, USA; [5]Institute of Chemistry & Biology of Membranes & Nanoobjects (UMR5248 CBMN), CNRS, Univ. Bordeaux, Institut Polytechnique Bordeaux, All. Geoffroy Saint-Hilaire, Pessac, France; [6]College of Life Sciences, Ritsumeikan University, Kusatsu, Japan; [7]Agroécologie, AgroSup Dijon, CNRS, INRA, Univ. Bourgogne Franche-Comté, Dijon, France; [8]Institut Laue-Langevin ILL, Grenoble, France; [9]Laboratoire de Biophysique Moléculaire aux Interfaces, TERRA Research Centre, GX ABT, Université de Liège, Gembloux, Belgium

Edited by Dennis Voelker

The plant plasma membrane (PM) is an essential barrier between the cell and the external environment, controlling signal perception and transmission. It consists of an asymmetrical lipid bilayer made up of three different lipid classes: sphingolipids, sterols, and phospholipids. The glycosyl inositol phosphoryl ceramides (GIPCs), representing up to 40% of total sphingolipids, are assumed to be almost exclusively in the outer leaflet of the PM. However, their biological role and properties are poorly defined. In this study, we investigated the role of GIPCs in membrane organization. Because GIPCs are not commercially available, we developed a protocol to extract and isolate GIPC-enriched fractions from eudicots (cauliflower and tobacco) and monocots (leek and rice). Lipidomic analysis confirmed the presence of trihydroxylated long chain bases and 2-hydroxylated very long-chain fatty acids up to 26 carbon atoms. The glycan head groups of the GIPCs from monocots and dicots were analyzed by gas chromatograph–mass spectrometry, revealing different sugar moieties. Multiple biophysics tools, namely Langmuir monolayer, ζ-Potential, light scattering, neutron reflectivity, solid state 2H-NMR, and molecular modeling, were used to investigate the physical properties of the GIPCs, as well as their interaction with free and conjugated phytosterols. We showed that GIPCs increase the thickness and electronegativity of model membranes, interact differentially with the different phytosterols species, and regulate the gel-to-fluid phase transition during temperature variations. These results unveil the multiple roles played by GIPCs in the plant PM.

The plant plasma membrane (PM) contains three main classes of lipids: phytosterols, sphingolipids, and phospholipids, all with a high level of molecular complexity, see (1, 2). Sphingolipids are part of essential lipids involved in the regulation of cellular signaling, trafficking, growth, and stress responses. Ubiquitous to eukaryotes, they are structurally different between the animal, fungi, and plant kingdoms (3). While some sphingolipid structures such as sphingoid bases are conserved in both plants and animal, others are specific to fungi and plants. In animal, sphingolipids are highly studied for their involvement in human health and pathologies (4). The most abundant sphingolipid in animal is sphingomyelin (SM) and gangliosides. In plants and fungi, they are absent, whereas other complex lipids comprised of sphingoid bases bound to glycan groups are part of the most abundant sphingolipid. The major sphingolipid subclass of sphingolipids in plants is the glycosyl inositol phosphoryl ceramides (GIPCs). GIPCs were discovered in plants and fungi during the 1950s (5). The structural diversity of GIPCs lies in the glycosylation and in the hydroxylation, degree and position of saturation of their fatty acid (FA) chain, and long chain base (LCB) (6). Plant GIPCs predominantly consist of a t18:0 or t18:1 LCB (trihydroxylated saturated or monounsaturated) amidified to a very long-chain fatty acid (VLCFA) or 2-hydroxylated VLCFA (hVLCFA) to form a ceramide (1, 7).

The GIPC head group linked to the ceramide consists of a phosphate bound to an inositol, forming the inositol phosphoryl ceramide (IPC) backbone, which is then further substituted with further sugar moieties. A broad study of the GIPC polar heads of 23 plant species from algae to monocots showed that polar head structures are largely unknown and vary widely across different biological taxa (8). GIPCs are classified into series, based on the degree of glycosylation of their polar head group (7). In plants, all GIPCs characterized to date have a glucuronic acid (GlcA) as the first sugar on the

* For correspondence: Sébastien Mongrand, sebastien.mongrand@u-bordeaux.fr.
Present address for Adiilah Mamode Cassim: Agroécologie, AgroSup Dijon, CNRS, INRA, Univ. Bourgogne Franche-Comté, Dijon F-21000, France.

IPC, followed by at least one more sugar unit of varying identity. For example, GIPC series A is defined as one monosaccharide addition to the GlcA-IPC form (7). In the 1960s, the first characterization of a GIPC structure from *Nicotiania tabacum* (tobacco) was described (9–58). The GIPC extraction method required hundreds of kilograms of plant material and liters of solvents. From the study, the reported series A GIPC still has the best described structure to date: GlcNAc(α1→4)GlcA(α1→2)inositol-1-O-phosphorylceramide, see Figure 1*A*. Additional sugar moieties were described, such as glucosamine (GlcN), *N*-acetyl-glucosamine (GlcNAc), arabinose (Ara), galactose (Gal), and mannose (Man), which may lead to observed glycan patterns of three to seven sugars, the so-called GIPC series B to F. It is noteworthy that Kaul and Lester calculated the ratio between carbohydrate/LCB/inositol in purified polyglycosylated GIPCs and showed that they may contain up to 19 to 20 sugars (12), which opens a very large field of investigation. Polyglycosylated GIPCs found in *Zea mays* (corn) seeds and *Erodium* display branched polar heads (13, 14). GIPC series are species- and tissue-specific. In Arabidopsis, the GIPC series A headgroup Man-GlcA-IPC is predominant in leaves and callus (15, 16), whereas a complex array of *N*-acetyl glycosylated with up to three pentose units are present in pollen (17). Amino-acylated and *N*-acylated GIPCs are found in Arabidopsis seeds and oil (18). GlcN(Ac)-GlcA-IPC is mainly found in rice and tobacco (7, 19). In monocots, the predominant GIPC series is series B (7), their core structures are yet to be deciphered.

The GIPC's polar head is responsible for the high polarity of the GIPC, accounting for its insolubility in traditional lipid extraction solvents, such as chloroform/methanol. Consequently, they are lost in the aqueous phase or at the interface.

A

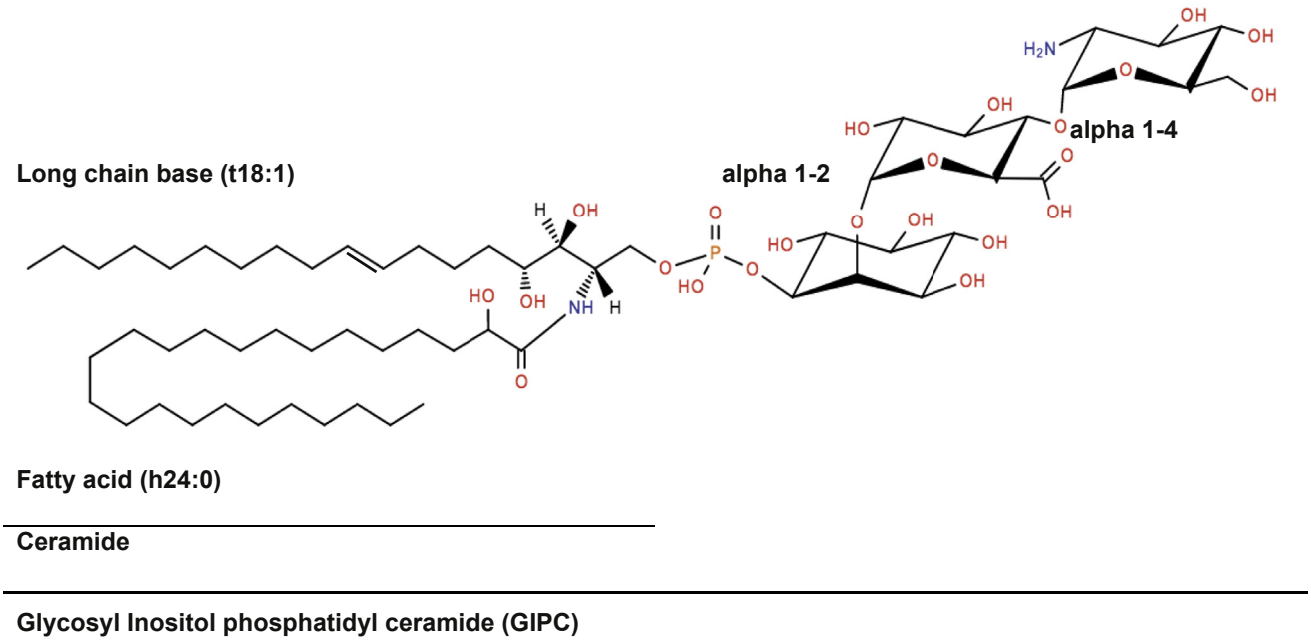

B

		Plant Species	Estimated GIPC by (h)VLCFA content (mg/g fw)	Main GIPC series as per Cacas et al., 2016
Eudicots	Plant (white parts)	*Brassica oleacera* (n=5)	4.3 ± 0.9	A
	Cell culture	*Nicotiana tabacum* (BY-2) (n=3)	0.6 ± 0.2	A B C D E F
Monocots	Plant (white parts)	*Allium porrum* (n=3)	0.4 ± 0.1	B
	Cell culture	*Oryza sativa* (n=3)	3.4 ± 0.2	B

Figure 1. Structure and amount of GIPC in plants. *A*, structure of GIPC series A (two sugars after the inositol group); *B*, GIPC content of different plant species: *Brassica oleracea* (cauliflower), *Nicotiana tabacum* (BY-2 cell culture), *Allium porrum* (leek), and *Oryza sativa* (rice cell culture). The GIPC content in mg per g of fresh weight was estimated by calculating the proportion of (h)VLCFA (hydroxylated very-long chain fatty acid) as determined by fatty acid methyl ester (GC-MS). The type of GIPC was defined by HPTLC analysis based on Cacas *et al.*, 2016 (1). Three to five independent samples were processed. Means ± SD are shown. GIPC, glycosyl inositol phosphoryl ceramide; HPTLC, high-performance thin-layer chromatography.

GIPCs, although one of the fundamental components of the plant PM model, have been poorly studied, in part because of the absence of commercial preparations. Recent evidence has demonstrated that a loss of the glycosylation is lethal (20, 21) and that misglycosylation affects both abiotic and biotic stress responses, as reviewed in (22). This highlighted the importance of investigating and understanding the chemical structures of these molecules and their functions in membrane organization.

Lipids are not homogeneously distributed within the PM bilayers. The lateral partitioning observed in the PM might be because of differential phase behaviors of different lipid species due to specific interactions between their different lipid species (23). This was reported in model membranes, using biophysical approaches and super resolution microscopy (24). Lipid domains or liquid-ordered (Lo) phases are formed from saturated phospholipids and sphingolipids in the presence of sterol, whereas liquid-disordered phases are formed mainly from unsaturated phospholipids (25, 26). In Lo phases, the high degree of conformational order is imposed on the acyl tails of lipids by the rigid ring structure of cholesterol. This increases the thickness of the lipid bilayer and lipid packing, although lipids remain laterally mobile (27). Sphingolipid-sterol interactions have recently been reported as important determinants of lipid partitioning and organization within the PM (28–30). The plant PM contains 20 to 50% sterols, depending on plant species and organ (31), harboring a wide molecular diversity including free and conjugated species and dominated by β-sitosterol, stigmasterol, and campesterol (32). These phytosterols play significant roles in differentially regulating the order level of the membrane such that ternary mixtures (sterol/sphingolipid/saturated phospholipid) have less temperature sensitivity to thermal variations compared with systems mimicking the lipid rafts of animal and fungi (30). β-sitosterol and campesterol have the largest effect on lipid ordering (1, 29, 30). Using environment-sensitive probes, it was shown that various phytosterols have the ability to modulate the proportion of Lo phases and membrane heterogeneity *in vivo* as *in vitro*, with the notable exception of stigmaterol (28, 29). Thus, GIPCs in synergy with sterols may organize and promote large-ordered domains such that both have important roles in PM subcompartmentalization and membrane dynamics (29).

In animal models, sphingolipids are involved in membrane organization and compartmentalization. Gangliosides, a ubiquitous glycosphingolipid found in all animal cell membrane, have a deep impact on membrane organization and the function of specific membrane proteins by influencing lipid–lipid and lipid–protein interactions within the external leaflet of the membrane (33). They interact with cholesterol to form raft (34). Both, animal gangliosides and plant GIPC, being in the outer membrane leaflet and their structural similarities such as long acyl chains and glycosylated head group, suggest that they may share related functions in membrane structure.

Here, we investigate the role of GIPC in membrane organization, we first aim at characterizing GIPC structural diversity, then proceed to understand how GIPC interacts with other membrane lipids, mainly sterols. To do so, it was fundamental to design a new protocol for the purification of GIPCs from different plant tissues and create model systems to characterize how GIPC alters membrane properties. As mentioned previously, older published protocols used large amounts of material and solvents, which is not feasible in modern labs. More recently, published protocols do not yield enough material of high enough purity for structural characterization. In this project, we devised a new protocol to obtain milligram amounts of highly enriched GIPC samples from both monocots and eudicots, suitable for use in studies of GIPC structure and its role in PM organization. Using biophysics tools such as Langmuir monolayers, molecular modeling, supported lipid bilayers, giant unilamellar vesicles (GUVs), dynamic light scattering (DLS), ζ-potential, cryo-electron microscopy (cryo-EM), solid state ^{2}H-NMR, and neutron reflectivity, we aim to uncover the role of GIPCs, in synergy with sterols, in the plant PM organization.

Results

Extraction and purification of GIPC-enriched fractions from different plant species tissues and cell culture

To assist with purifying the milligram amount of GIPCs required for analysis, we first assessed the amount of GIPCs in different plant species and tissues. We chose species/tissues which are easily and abundantly available and quantified the nonhydroxylated VLCFA and 2-hydroxylated hVLCFA, diagnostic of plant GIPC (1). Four species were selected to get different GIPC series: two eudicot plants: cauliflower (*Brassica oleacera, Bo*) head and tobacco (*Nicotiana tabacum, Nt*) cell culture Bright-Yellow 2 (BY-2) and two monocot plants: the white leaves of leek (*Allium porrum, Ap*) and rice (*Oryza sativa, Oz*) cell culture. The white part of plant tissues and cell cultures were used to avoid contamination by the abundant plastidial lipids and pigments. Cauliflower and rice cell culture have the highest GIPC content with an estimated 4.3 mg/ml and 3.4 mg/ml per fresh weight, respectively (Fig. 1*B*). BY2 cells and leek both had a much lower GIPC content, with a mean estimated content of 0.6 mg/ml and 0.4 mg/ml per fresh weight, respectively.

To maximize the yield, several trials were performed to test the different published protocols of GIPCs (11, 12, 35). Figure 2 shows the extraction and purification processes selected combining the most efficient steps of each of these protocols to obtain GIPC-enriched fractions of cauliflower (Bo-GIPC), tobacco BY-2 (Nt-GIPC), leek (Ap-GIPC), and rice (Os-GIPC). Some fine-tuning was done to maximize the yield such as refluxing in boiling ethanol for 20 min and using large lab-made silica column to process several hundreds of grams of material (see Experimental procedures). Crude sphingolipid extracts were directly dried in silica deposited on the top of the column chromatography. The column was then washed with four column volumes (cv) of a mix of chloroform/methanol with increasing polarity to remove sterols, glucosylceramide, and phospholipids. For the elution of GIPCs, a step gradient of chloroform/methanol/water was used (Fig. 2*A*), so that

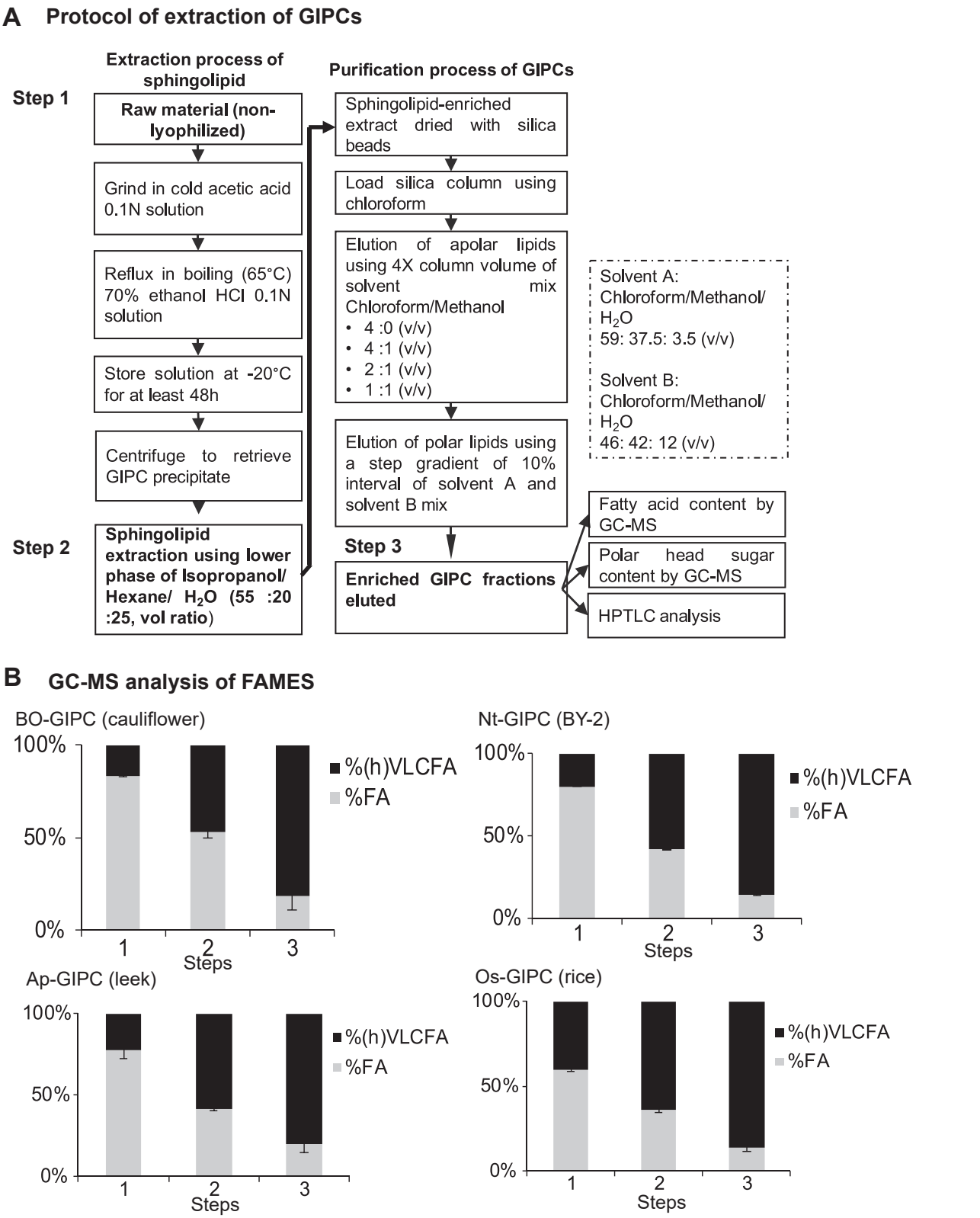

Figure 2. Extraction and purification protocol of GIPCs. *A*, GIPC purification scheme, adapted from (11, 12, 35). The three steps 1, 2, and 3, respectively, are important milestones in the GIPC isolation steps; *B*, gas chromatography-mass spectrometry (GC-MS) analysis of fatty acid content after steps 1, 2, and 3 of the extraction and purification process. Aliquots of *Bo*-cauliflower, *Nt*-BY-2, *Ap*-leek, and *Os*-rice samples at step 1, 2, and 3 underwent transmethylation to release fatty acid before derivatization by BSTFA, and the resulting FAMES were analyzed by GC-MS and the fatty acid content calculated. FA refer to fatty acid of 16 to 18 carbon atoms fatty acids and (h)VLCFA refer to hydroxylated or nonhydroxylated very long chain fatty acid of 20 to 28 carbon atoms. The amount of GIPC in each sample were extrapolated from the (h)VLCFA content. Data shown for three independent replicas. Error bars are SD. BSTFA, N,O-Bis(triméthylsilyl)trifluoroacetamide; FA, fatty acid; FAMES, fatty acid methyl esters; GIPC, glycosyl inositol phosphoryl ceramide; HPTLC, high-performance thin-layer chromatography.

molecules of increasing polarity were eluted in the last fractions. All washes and elution fractions were collected and analyzed by high-performance thin layer chromatography (HPTLC) as shown in Data S1. HPTLC was a quick and reliable way to select fractions enriched with GIPCs, because it allowed the clear separation of sterols, phospholipids, and GIPC series.

Fatty acid content of GIPC-enriched fractions

To estimate the GIPC content, as well as the phospholipid contamination (containing medium chain fatty acid FA of C16–18), samples were trans-esterified to release both fatty acid-esterified glycerolipids and fatty acid-amidified sphingolipids. The samples were then analyzed by gas chromatograph–mass spectrometry (GC-MS). The percentage of fatty acid in the samples with medium chain length (%FA) and hydroxylated and nonhydroxylated very long chain length (%(h)VLCFA) were calculated from two to three independent experiments. Samples retained after step 1 (raw plant material), step 2 (crude sphingolipid extract), and step 3 (GIPC-enriched fractions) were analyzed for their fatty acid content. As we proceeded through the purification steps, the amount of medium chain FA decreased as the amount of (h)VLCFA increased (Fig. 2*B*). At step 2, the percentage of (h)VLVCFA in the sphingolipid extract was around 50%, and at the final step, the amount of (h)VLCFA was at about 80% for all GIPC-enriched extracts (Fig. 2, *A* and *B*). The detailed FA composition of the GIPC-enriched fractions of all four species is provided in Data S2. It was estimated that the enrichment in GIPC between the first and last steps of the extraction and purification process was 5-fold for Bo-GIPC, 4.2-fold for Nt-GIPC, 3.6-fold for Ap-GIPC but only 2-fold for Os-GIPC.

The final products were analyzed by HPTLC to verify the lipid composition, and they revealed the predominance of GIPCs (Fig. 3). Only traces of sterols and phospholipids were observed, and glucosylceramide (GluCer) was not detected. As reported in (7), eudicots contained mainly series A, monocots series B, and plant cells in liquid culture media, a mix of GIPCs with highly glycosylated ones. The Bo-GIPC–enriched fraction contained one major band of GIPC series A. The Nt-GIPC fraction contained GIPC series A to F, further separated into three fractions (α, β, and γ) of increasing polarity. The less polar fraction α contained two bands of series A GIPC closely packed together, representing PhytoSphingoLipid 1, PSL1 (with *N*-acetyl glucosamine), and PSL2 (with GlcN) as described in (12) (Fig. 3) and a band of series B. The more polar fractions β and γ showed the presence of the highly polyglycosylated D to F series GIPC (Fig. 3). As previously

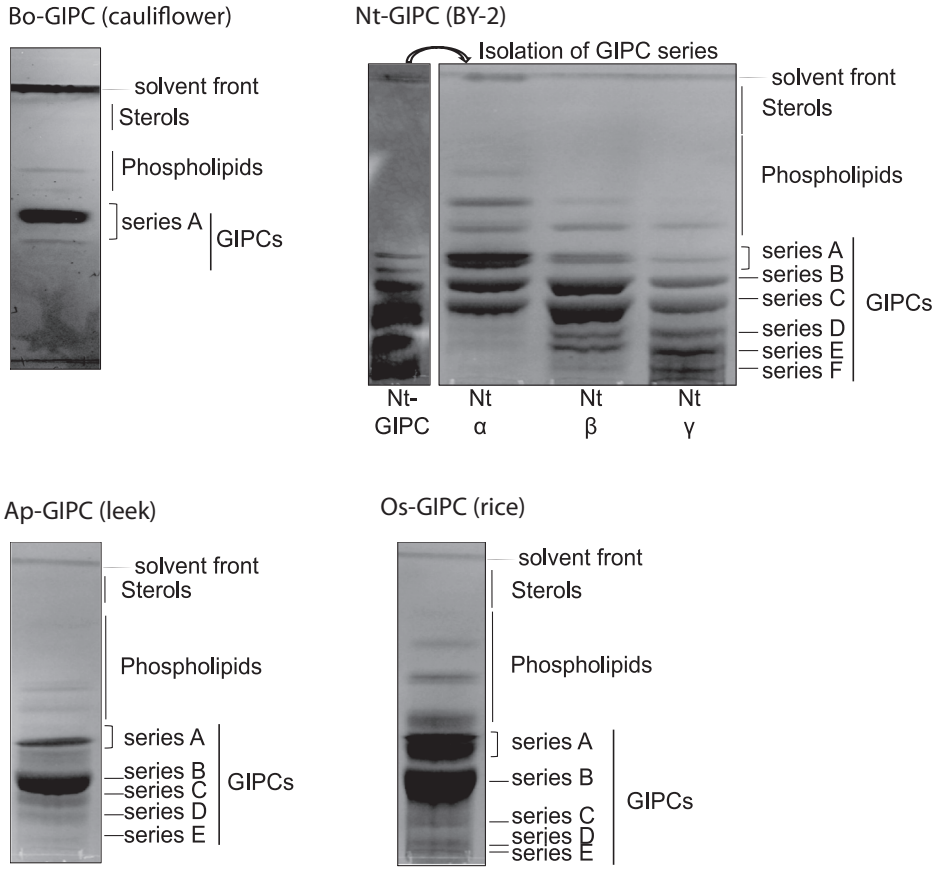

Figure 3. High-performance thin layer chromatography analysis during silica column purification. High-performance thin layer chromatography shows the GIPC content after purification step 3, described in Figure 2. Bo-GIPC purified from cauliflower contains mainly series A. Tobacco cell culture BY-2 (Nt-GIPC) sample were further separated by column chromatography to isolate the different GIPC series. Fraction α contains mainly series A, B, and C, whereas fractions β and γ show presence of polyglycosylated GIPCs (series D, E, F, etc). Ap-GIPC purified from leek and Os-GIPC purified from rice samples contain mainly GIPC series B. GIPC, glycosyl inositol phosphoryl ceramide.

published monocots, Ap-GIPC– and Os-GIPC–enriched fractions contained mainly GIPC series B, some series A and to a lesser extent polyglycosylated GIPCs also present.

Regarding GIPC-derived (h)VLCFA, the predominant species was dependent on the starting material. The Bo-GIPC enriched fraction consisted of h24, h24:1, and h26 as the main fatty acyl chain, Nt-GIPC with h22, h23, h24, and h25 acyl chain, Ap-GIPC with C24, h24, h22 and C22 and Os-GIPC with C24, C22, C20, and h24 (Fig. 4*A*).

We next investigated the sugar moieties present in GIPC-enriched fractions by high-performance anion exchange chromatography coupled with pulsed amperometric detection, a technique used to detect underivatized monosaccharide sugars (Data S3). Control experiments showed that acid hydrolysis has no to very little effect on the sugar moieties of GIPC fractions (Data S4). As expected, all GIPC-enriched fractions contained GlcA found in GIPC samples previously characterized, see for review (36). The Bo-GIPC enriched fraction not only contains glucose (Glc) and Man previously found in Brassicaceae species (16) but also large amount of Ara and Gal. These latter sugars, never described in Brassicaceae such as Arabidopsis, could be a real specificity of Bo-GIPC's polar head or due to cell wall/glycoprotein contamination of the GIPC-enriched fraction, see further below.

The different fractions of the Nt-GIPC series have a complex glycan content. Fraction α contained GlcA, GlcN, and Man (Data S3). Note here that GlcNAc is hydrolyzed during the extraction procedure and is mixed with GlcN. Gal and Ara became the main glycan moieties in fractions β and γ as described for highly glycosylated GIPC, series D (59). Monocot GIPC-enriched sample, both Ap-GIPC and Os-GIPC, contained mainly Man, Gal, and GlcN at relatively equal amount, and GlcA and Ara at lower amount (Data S3).

Previous studies have suggested interactions between GIPCs and cell wall components, particularly the pectin Rhamnogalacturonan II (37). However, we did not detect either galacturonic acid nor rhamnose, two main components of pectins, suggesting no major pectin contamination (Fig. 4*B*). We detected, however, a large amount of Ara and Gal (Data S3). A Yariv reactivity test (38) was performed to check for

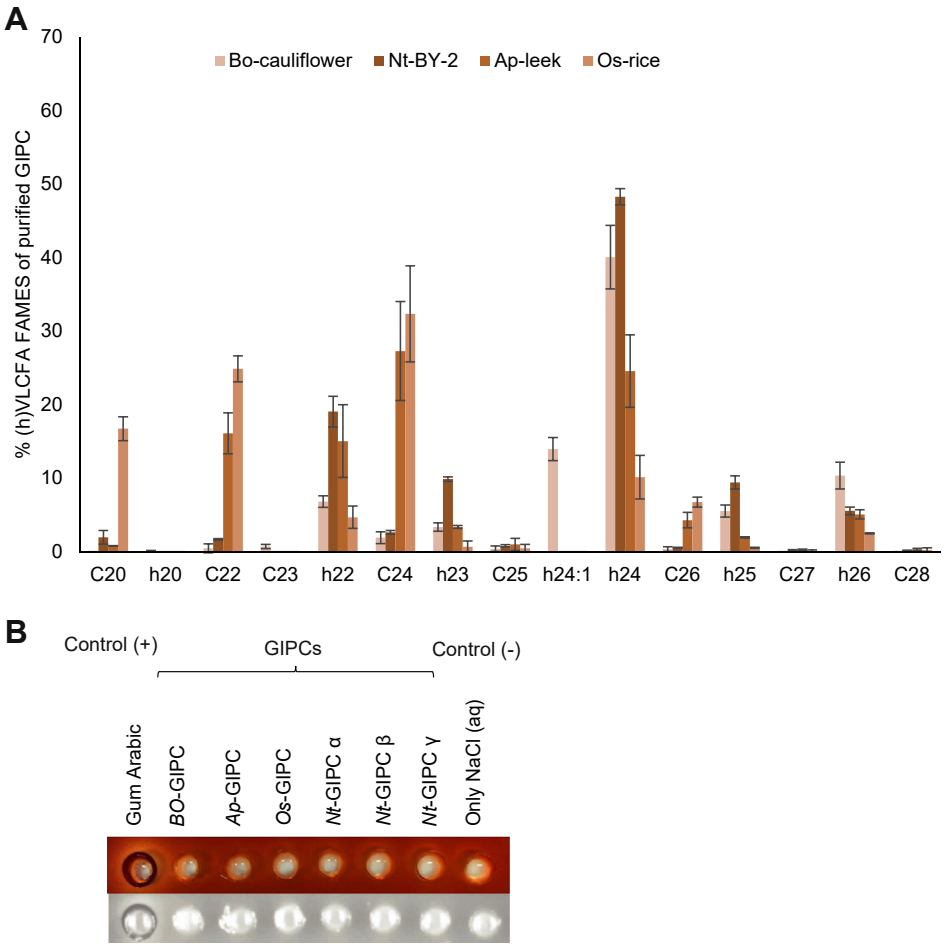

Figure 4. Fatty acid content of GIPC-enriched samples. *A*, very long-chain fatty acid (VLCFA) and hydroxylated VLCFA (hVLCFA) content of GIPC-enriched samples from cauliflower, BY-2 cell culture, leek and rice cell culture. The fatty acids were released from the GIPC-enriched samples by transmethylation followed by derivatization using BSTFA, before GC-MS analysis. Four to six independent samples were analyzed. Means ± SD are shown. *B*, Yariv reactivity test of GIPC-enriched samples to detect arabino-galactan content. No arabino-galactan were detected. 50 µg of each sample (1 mg/ml) was deposited in each well, and the picture was taken 48 h after initiating the reaction. BSTFA, N,O-Bis(triméthylsilyl)trifluoroacetamide; GIPC, glycosyl inositol phosphoryl ceramide.

the presence the arabino-galactan as contaminants in the GIPC-enriched fractions (Fig. 4*B*). No zone of clearance was observed, suggesting no detectable arabino-galactan in each GIPC sample (50 μg). Gum arabic and saline buffer were used as positive and negative controls, respectively (Fig. 4*B*). The potential contamination of the GIPC samples by proteins was also tested using the Bradford method. However, in GIPC samples of up to 30 μg, no protein was detected (data not shown).

The highly purified fractions of Bo-GIPC and Ap-GIPC were analyzed by LC-MS (2) in MRM mode and compared with total sphingolipids extracted from crude cauliflower or crude leek. Results showed in Data S4 revealed an absence of CER and GluCer contamination in the purified GIPC sample and that the LCB and FA content is very similar except a slight loss of h24:0/1- and t18:0/1-containing GIPC (less than 10%), see Data S5.

Biophysical characterization of the GIPC-sterol interaction

We decided to focus on the Bo-GIPC preparation to perform various biophysical analyses to obtain elements of understanding on how GIPCs molecular characteristics contribute to the organization of the plant PM. We first characterized the lipid–lipid interactions at the micrometric level by the Langmuir trough compression technique applied on a monolayer model at the air–water interface (39). The interaction of Bo-GIPC with free and conjugated sterols (β-sitosteryl glucoside, steryl glucoside [SG], and acyl (18:2) β-sitosteryl glucoside, ASG). The ratio of GIPC:sterol (80:20 mol ratio) is consistent with the estimated ratio of the lipids in the outer leaflet of the PM (1, 40). The compression isotherm of Bo-GIPC (green line) (Fig. 5*A*) shows a low and relatively constant surface pressure in large molecular areas, corresponding to a "gaseous" state. Compression of the monolayer induced a progressive increase in surface pressure, indicating the appearance of a liquid-expanded state (in agreement with the two-dimensional compressibility modulus, Cs^{-1}, of 38.3 mN m^{-1} in the 160- to 110- $Å^2$ per molecular region), which is characterized by a certain degree of condensing interaction between the molecules at the interface (Fig. 5*A*). The mean interfacial area of Bo-GIPC is 212.9 ± 4.9 $Å^2$ in its expanded form and at its most condensed form is 60.0 ± 14.6 $Å^2$. These results are in agreement with the results previously obtained with *Nicotiana tabaccum*-GIPCs (1).

The interaction of Bo-GIPC mixed with different sterols was assessed by the thermodynamic analysis of the compression isotherms of mixed GIPC-sterol monolayers. In this comparative study, we adhere to the rule of additivity, which suggests that if two molecules within a mixed monolayer are immiscible, the area occupied by the mixed film will be the sum of the areas of the separated components. The deviation to that rule is attributed to the existence of specific interaction between the two molecules (41). The mean molecular area of the mixed monolayer Bo-GIPC: β-sitosterol (80:20) was lower than the calculated theoretical value (using the rule of additivity), at the estimated physiological membrane surface pressure of 30 mN m^{-1} (42) (Fig. 5*B*). This condensing effect of β-sitosterol in presence of Bo-GIPC confirms that previously reported for tobacco GIPCs (1). This trend was however reversed for the mixed monolayers of Bo-GIPC:SG (80:20) and Bo-GIPC:stigmasterol (80:20), where the mean molecular area is significantly higher than the theoretical value (Fig. 5*B*). For Bo-GIPC:ASG (80:20), the effect is intermediate. The most significant difference between the experimental and theoretical mean molecular area was obtained for the mixed monolayer Bo-GIPC:stigmasterol (80:20). Interestingly, the only structural difference between β-sitosterol and stigmasterol is the presence of a double bond at C22 in stigmasterol. The mixed monolayer GIPC:ASG (80:20) had a comparable mean molecular area to GIPC molecule at low surface area (Fig. 5*A*), and the average difference between the mean molecular area and its theoretical value is 30 $Å^2$ per molecule for all three surface pressures (Fig. 5*B*).

To thermodynamically analyze the interaction of the two components and the stability of the mixed monolayer, the excess free energy of the mixing (ΔGex) and the free energy of mixing (ΔGM) were respectively calculated for all four mixed monolayers (Fig. 5*C*). The negative value of ΔGex for the mixed monolayer GIPC: β-sitosterol (80:20) suggested a strong attractive interaction between the two components, and the negative value of ΔGM indicated thermodynamic stability of the mixed monolayer (Fig. 5*C*) as suggested by (1). The values of ΔGex and of ΔGM for the mixed monolayers GIPC:SG (80:20), GIPC:ASG (80:20), and GIPC/Stigmasterol (80:20) were both positive in all three mixed monolayers (Fig. 5*C*) showing repulsion between the molecules within the monolayer and thermodynamic instability of the mixed monolayers.

Modeling the interaction between GIPC and phytosterols

The interaction of one molecule of GIPC series A with t18:0/h24:0 and one molecule of sterol was generated *in silico* and analyzed using Hypermatrix, a simple docking method used to calculate specific interactions between two amphiphilic molecules (for a review see (39)). The sterols used were the four molecules studied by the Langmuir monolayer technique, *i.e.*, β-sitosterol, stigmasterol, ASG, and SG (Fig. 6). The interacting molecules displayed very different configurations. The differences between the spatial organization of the GIPC/sitosterol and GIPC/stigmasterol were striking: the α-side of the steryl moieties of β-sitosterol was directed toward the acyl chains of the GIPC, whereas the steryl rings of stigmasterol was positioned at a perpendicular angle with respect to GIPC hydrocarbon chains (Fig. 6, *A* and *B*). In mammals, the interaction of the α face of cholesterol with lipid acyl chains favors its condensing effect (43). This was notably established by comparing the effects of cholesterol and lanosterol, which possesses a methyl group on the α face, on lipid organization (44–46). For stigmasterol, the structural difference of the unsaturation on C22 seems thus to modify its interaction with GIPC (Fig. 6*B*), and this can be correlated to the non-condensing effect observed experimentally in the monolayer compression experiments (Fig. 5). Similarly, the β face of the

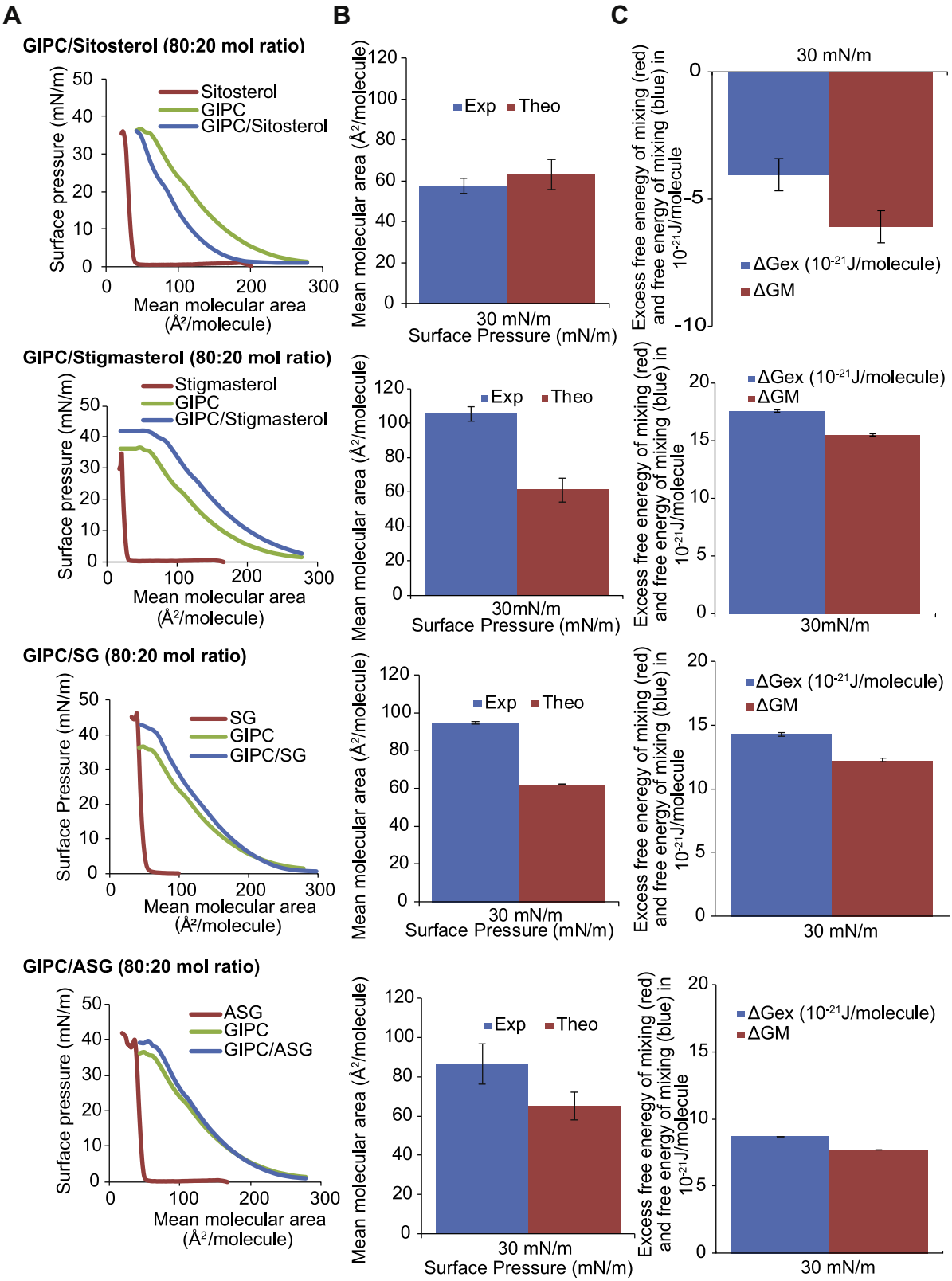

Figure 5. Study of the interaction of GIPC and phytosterols in Langmuir monolayer. *A*, surface pressure-area (π-A) isotherms, at the air-aqueous phase interface, of pure GIPC and sterol monolayers and of mixed GIPC/sterol monolayer prepared at a molar ratio of 0.80. The isotherms were recorded at 25 °C on an aqueous subphase composed by 10 mM Tris buffer at pH 7. Each compression isotherm is representative of at least two independent experiments, each of them repeated at least three times. *B*, comparison of the experimental (*blue bars*) and theoretical (*red bars*) mean molecular areas at a surface pressure of 30 mN/m for a GIPC/sterol molar ratio of 0.80. The theoretical value is obtained according to the additivity rule: $A_{12} = A_1X_1 + A_2X_2$, where A_{12} is the mean molecular area for ideal mixing of the two components at a given π, A_1 and A_2 are the molecular areas of the respective components in their pure monolayers at the same π, and X_1 and X_2 are the molar ratios of components 1 and 2 in the mixed monolayers. Data are from at least six experiments; Means ± SD are shown; *C*, excess free energy of mixing (ΔGex; *blue bars*) and free energy of mixing (ΔGM; *red bars*) of the mixed monolayer GIPC/sterol at a molar ratio of 0.80 at the surface pressure of 30 mN/m. ΔGex and ΔGM were calculated according to the equations as shown in (41, 77). Data are from at least six experiments; Means ± SD are shown. ASG, acyl steryl glucoside (sitosterol, glucose head group, and C18:2 acyl chain); GIPC, glycosyl inositol phosphoryl ceramide; SG, steryl glucoside (sitosterol, glucose head group).

steryl ring moiety of the SG was oriented toward GIPC acyl chains. It is noteworthy that the bending of the sugar head group of GIPC favors its interaction with the Glc head group of SG (Fig. 6*C*). In the conformation of the conjugated sterol ASG, the acyl chain is in direct interaction with the α side of the sterol, such that the β-side of the steryl cycle interacts with GIPC acyl chains (Fig. 6*B*). Thus, β-sitosterol is the only sterol tested for which the interaction of its α-face with the GIPC acyl chains is favored, in good agreement with its condensing effects observed experimentally.

Effect of GIPC on membrane organization and thickness

To further investigate the properties of GIPC in influencing plant PM organization, we used Bo-GIPC to make large unilamellar vesicles (LUVs) by freeze/thawing method. GIPC alone made aggregates but not vesicles (Fig. 7*A*). Phase contrast microscopy observations of Nt-GIPC containing LUV in water at RT, pH 7, led to similar results (Data S6*A*). However, by adding phospholipids, we could observe the formation of LUV (Data S5*A*). To closely mimic the outer leaflet of the PM enriched in GIPCs, we generated LUV with a ternary system of GIPC:phospholipid:β-sitosterol (1:1:1). For all phospholipids used, *i.e.*, 1-palmitoyl-2-linoleoyl-*sn*-glycero-3-phosphocholine (PLPC), 1-palmitoyl-2-oleoyl-*sn*-glycero-3-phosphocholine (POPC), or dioleoyl-*sn*-glycero-3-phosphocholine (DOPC), the ternary system yielded liposomes using the freeze-thaw method (Fig. 7*A*) (Data S6*B*). GUVs were also made using the Teflon method (47) with a ternary mix of GIPC/DOPC/sitosterol (Fig. 7*B*). GIPC cannot organize alone in bilayer but need phospholipids and sterols.

The incorporation of GIPCs into the liposomes were analyzed by DLS which gives the hydrodynamic diameter of the liposomes. The addition of GIPC did not seem to affect the hydrodynamic diameter of liposomes, which was about 100 nm.

The structure of the LUVs made by the freeze/thaw method was further investigated by cryo-EM. GIPC/POPC-(2)H_{31}/β-sitosterol- and GIPC/POPC-(2)H_{31}/stigmasterol-containing LUVs formed not only regular-shaped bilayer vesicles but also planar bilayer structures that seem more rigid and not able to bend and make proper vesicles (arrow in Fig. 8*A*).

Comparison of the bilayer thickness of these GIPC-containing LUVs with LUVs containing only POPC and sterols showed a significant difference of thickness from 4.5 nm for the ternary LUV to 3.5 for the binary LUV (Fig. 8*B*). We also investigated the influence of GIPCs on membrane thickness by neutron reflectivity (Fig. 9*A*). Supported lipid bilayers (SLBs) were formed by vesicle fusion of liposomes containing POPC, GIPC, and constant β-sitosterol concentration. Three different membrane compositions were tested with increasing (0, 15, and 30% mol.) GIPC concentration. The reflectivity profile was analyzed, and following model fitting, the scattering length density profile and the thickness of the polar head and acyl tail in the bilayer were obtained. The results showed that liposomes containing 30% mol of GIPC did not form a continuous bilayer on the surface, as indicated by a high solvent content in the hydrophobic tail region. This implies that the high GIPC content modified the bilayer properties, such that it did not adhere to the support. However, 0 and 15% mol containing GIPC liposomes did form continuous bilayers. The addition of GIPCs increased the bilayer thickness by 8 Å, as compared with GIPC-free SLBs, because of the 4 Å of sugar head group in each layer (Fig. 9*A*). Refer to the tables of Figure 9*B* for more details of the structural parameters that were generated. Figure 9*C* shows an overlay of the estimated SLB dimensions on the scattering length density profile of the SLBs.

The ζ-potential of the GIPC-containing liposomes was measured to be around −26 mV, whereas DOPC/β-sitosterol alone had a ζ-potential of −5 mV (Fig. 7*C*). The difference in ζ-potential between GIPC and GIPC-free liposomes is attributed to the fact that GIPCs are negatively charged because of the presence of the glucuronic acid and furthermore confirms that GIPC was indeed incorporated into the lipid membrane (48) and showed that the ζ-potential of the surface of wild-type *Arabidopsis* mesophyll cells are at −20 mV which is quite close to that of our liposomes. It seems that GIPC contributes significantly to the negative potential of the plant PM outer leaflet, which might influence, for example, its interaction with cell wall components.

Effect of GIPC on membrane biophysical properties

Finally, we asked whether GIPCs have an effect on the gel-to-fluid phase transition of a fully hydrated binary and ternary lipid mix system using solid-state ^{2}H-NMR spectroscopy as a nonintrusive method giving structural and dynamic information about lipid bilayers (49, 50). Here, we aimed to find the nature of the membrane phases, their dynamics, and how GIPCs and phytosterols are regulating the membrane phase transition, such as the well-described effect of cholesterol on the membrane (51).

We used Bo-GIPC–enriched fractions to make membrane systems using deuterated palmitoyl-oleoyl phosphatidylcholine containing 31 atoms of deuterium on the palmitoyl chain (POPC-(2)H_{31}) as a probe for solid-state ^{2}H-NMR. We chose to use POPC as it is a phospholipid with a long chain fatty acid with an unsaturation found in plant PM (1) and a gel-to-fluid transition temperature of −2.5 °C ± 2.4 deg. C (52). We generated liposomes using the freeze/thaw method as previously described. Figure 10*A* showed ^{2}H NMR spectra of two lipid mix systems containing GIPC (GIPC/POPC-(2)H_{31}/β-sitosterol (1:1:1, mol ratio) and GIPC/POPC-(2)H_{31}/stigmasterol (1:1:1, mol ratio)) and two control samples without GIPC (POPC-(2)H_{31}/β-sitosterol (1:1, mol ratio) and POPC-(2)H_{31}/stigmasterol (1:1, mol ratio)). Spectra were acquired by varying the temperature from −10 to 40 °C, corresponding to plausible thermal variations that plants may experience in nature. The obtained ^{2}H NMR spectra exhibit the typical powder pattern line shape with a spectral width decreasing as the temperatures increase. This qualitative observation can be supplemented by a quantitative characterization using the first spectral moment (50). Figure 10*B* shows the temperature plots of first moments

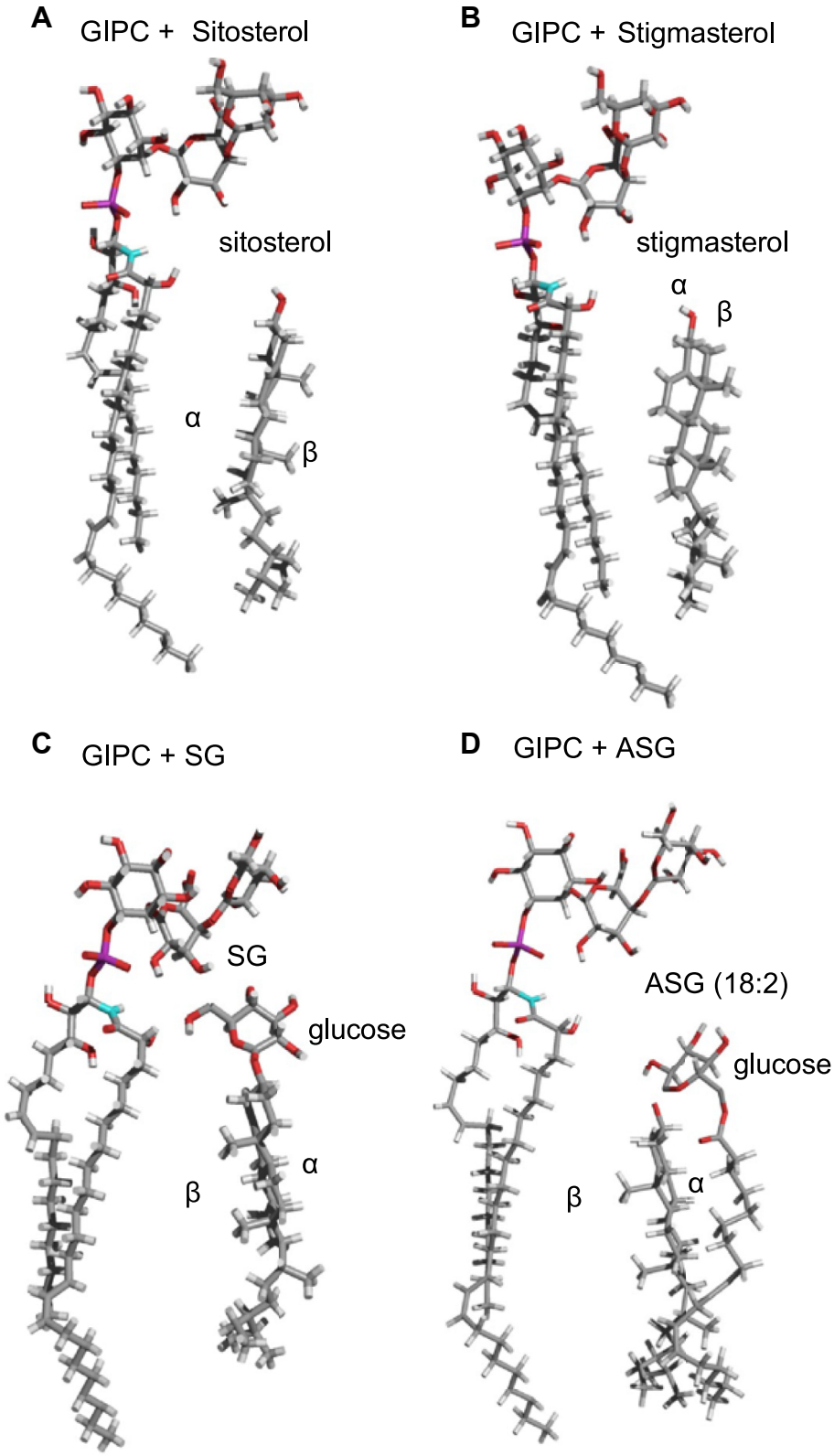

Figure 6. Modeling of the interaction between GIPC and sterols. Theoretical interactions calculated by HyperMatrix docking method with one molecule of GIPC series A t18:0/h24:0 and one molecule of either *A*, β-sitosterol or *B*, stigmasterol or *C*, steryl Glucoside, SG (β-sitosterol, with glucose head group), or *D*, acyl steryl glucoside, ASG (β-sitosterol, with glucose head group/18:2 acyl chain). GIPC, glycosyl inositol phosphoryl ceramide.

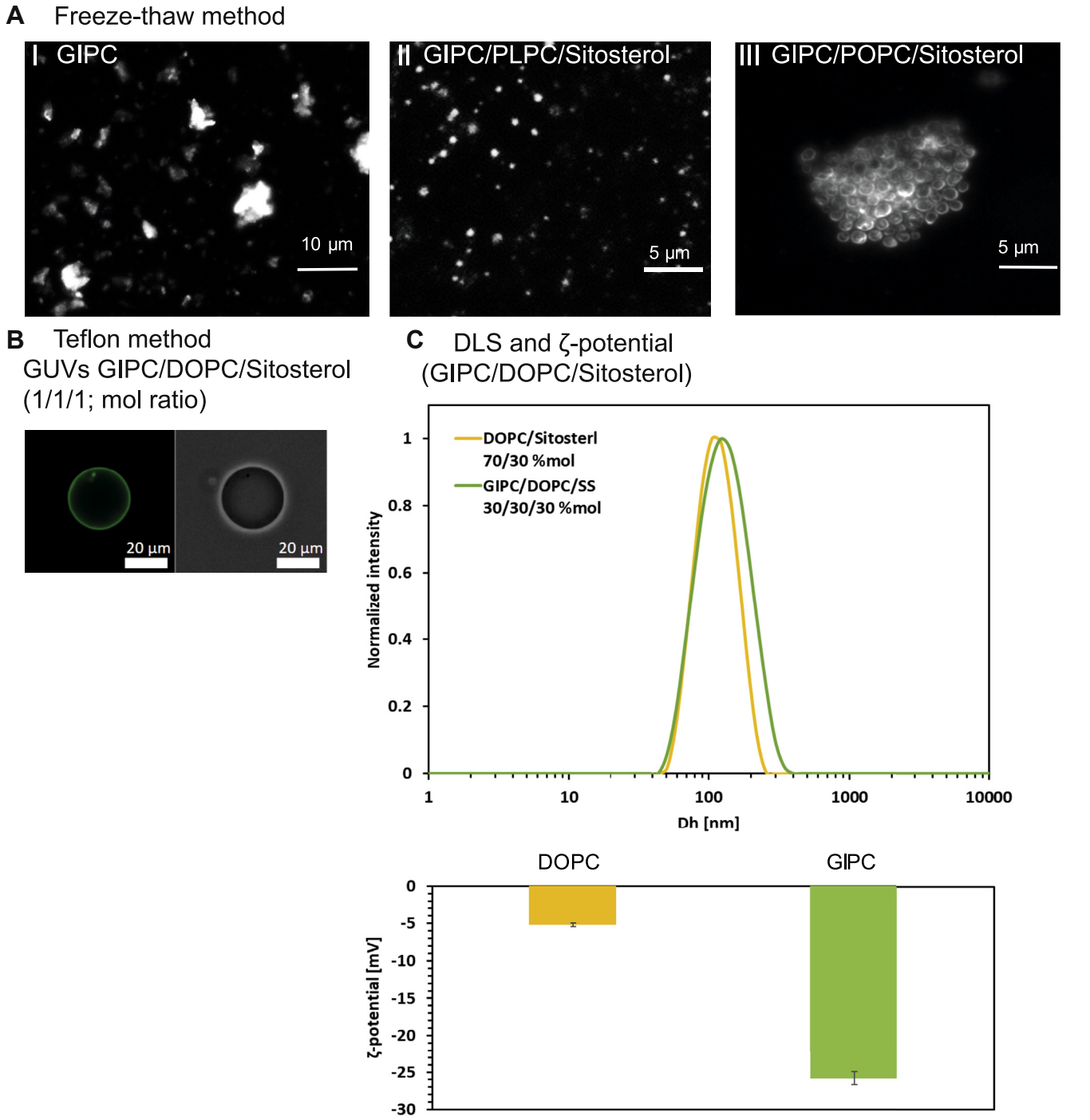

Figure 7. Study of GIPC containing-liposomes in binary and ternary. *A*, phase contrast microscopy images of Bo-GIPC containing-liposomes in buffer solution after three cycles of freeze and thaw. Enriched Bo-GIPC (cauliflower) underwent freeze (−20 °C, 20 min) and thaw (60 °C, 20 min) cycles three times GIPC in TBS buffer pH 5.8 with or without phospholipid and β-sitosterol at a concentration of 1 mg/ml. (I) GIPCs alone form crystals in a saline buffer solution. A lipid mix, at a concentration of 1 mg/ml, of GIPC/PLPC/β-sitosterol or GIPC/POPC/β-sitosterol (1:1:1, mol/mol), shown in (II) and (III) respectively, forms vesicles of approx. 2 µm. *B*, fluorescence and phase contrast microscopy images of Giant unilamellar vesicles (GUVs) of GIPC/DOPC/β-sitosterol (1:1:1, mol/mol). The lipid mix was labeled by NBD-PC at 0.1% mol. *C*, dynamic light scattering (DLS) and ζ-potential of liposomes containing DOPC/β-sitosterol (7:3, mol ratio) (*yellow*) and GIPC/DOPC/β-sitosterol (1:1:1, mol ratio) (*green*), respectively, provide the size which is around 100 nm and ζ-potential values of −28 mV in the presence of GIPC. Three to four replica using independent GIPC purification was measured. Means ± SD are shown. DOPC, dioleoyl-*sn*-glycero-3-phosphocholine; GIPC, glycosyl inositol phosphoryl ceramide; NBD-PC, 1-palmitoyl-2-{6-[(7-nitro-2-1,3-benzoxadiazol-4-yl) amino]hexanoyl}-sn-glycero-3-phosphocholine.

(M1) calculated from ^{2}H-NMR powder spectra of liposomes with or without Bo-GIPCs, as well as pure POPC-(2)H_{31}. On Figure 10*B left*, we can hence appreciate the phase transition of a pure POPC-(2)H_{31} membrane such that the low M1 corresponds to the fluid (*Ld*) phase and the high M1 to the rigid (*Lo*) phase. The thermal variation showed an abolished phase

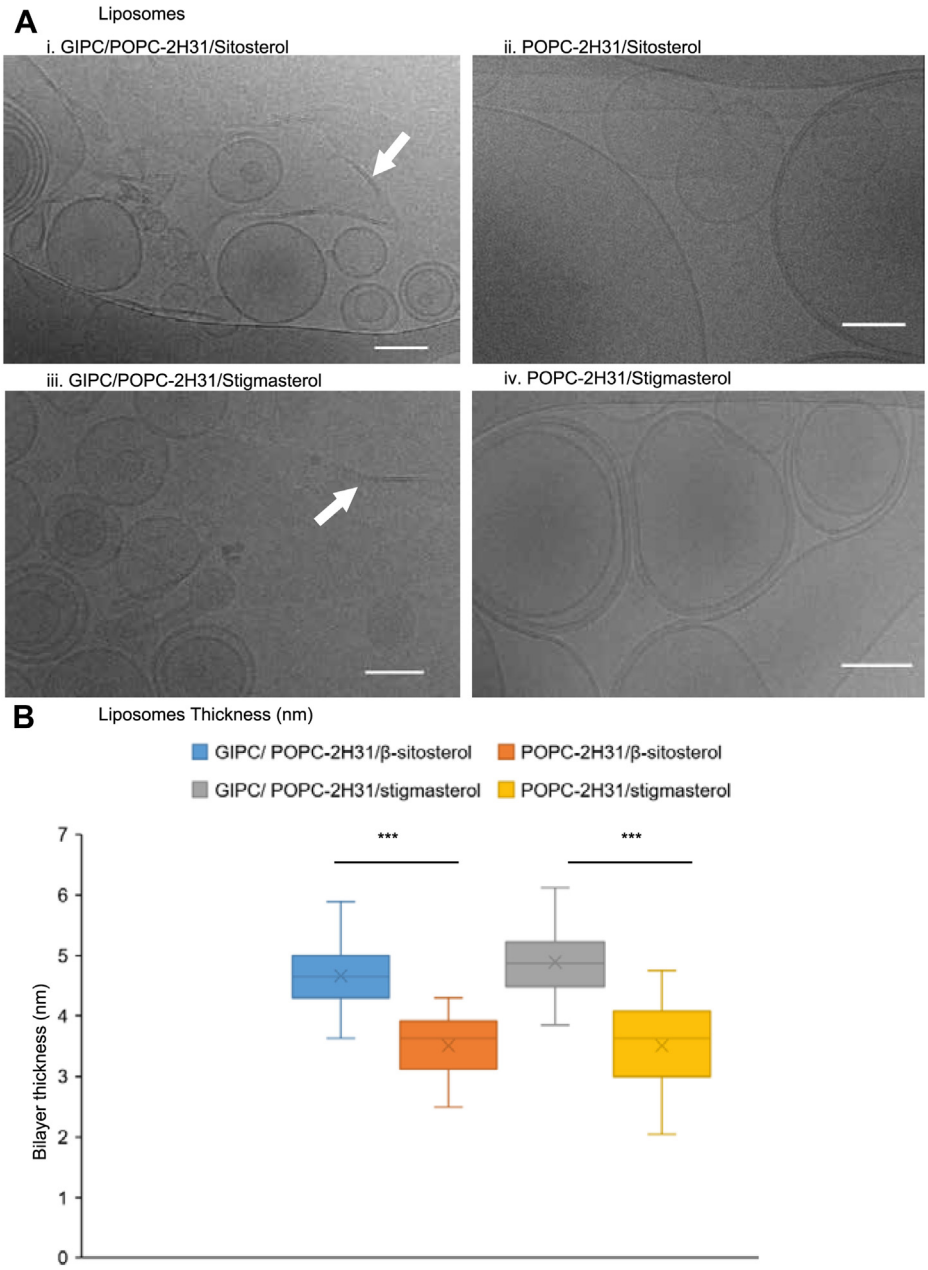

Figure 8. Membrane thickness vary with the presence of GIPC. *A*, cryo-EM images of liposomes. POPC-d31 that is a deuterated POPC on the carbon of the palmitoyl chain: 16:0-d31 to 18:1 PC, in the presence of sterols (ii: sitosterol and iv: stigmasterol) are mainly present as vesicles, showing one to few bilayers. In the presence of GIPC, these liposomes are still observed, but at the same time, rigid bilayers structures appearing as flat entities are also observed (*white arrows* in i and iii). Scale bar, 100 nm; *B*, membrane thickness measurements. Measurements were made using ImageJ software to compare the membrane thickness with or without GIPC. For each lipid system, the width of the bilayer was measured in two different ROI per liposomes in ten independent liposomes from two different cryoEM grids. Error bars are SD (n = 20). Significance was determined by Student's *t* test. ***$p < 0.0001$. cryo-EM, cryo-electron microscopy; GIPC, glycosyl inositol phosphoryl ceramide; POPC, 1-palmitoyl-2-oleoyl-*sn*-glycero-3-phosphocholine.

transition upon adding phytosterols to POPC-(2)H_{31} (Fig. 10*B left*). This abolition is more pronounced for β-sitosterol with a higher ordering effect above the phase transition temperature compared with stigmasterol. These conclusions can be transposed to ternary systems with the difference that β-sitosterol has a stiffening effect at low temperatures (Fig. 10*B right*). Above the POPC-(2)H_{31} phase transition, both GIPC and phytosterol were able to rigidify the membrane, with a larger effect for β-sitosterol. This result is similar to those obtained by Beck *et al.*, 2007 (30). Taken together, these experiments showed that GIPC and phytosterols adopt the same behavior as cholesterol and hence have a high propensity to regulate fluidity during temperature variations.

Discussion

Fine-tuning GIPC purification

GIPCs are essential components of plant PMs (8, 15). As there are no commercially available GIPCs, reasonable quantities of these molecules must be isolated with good purity to

A

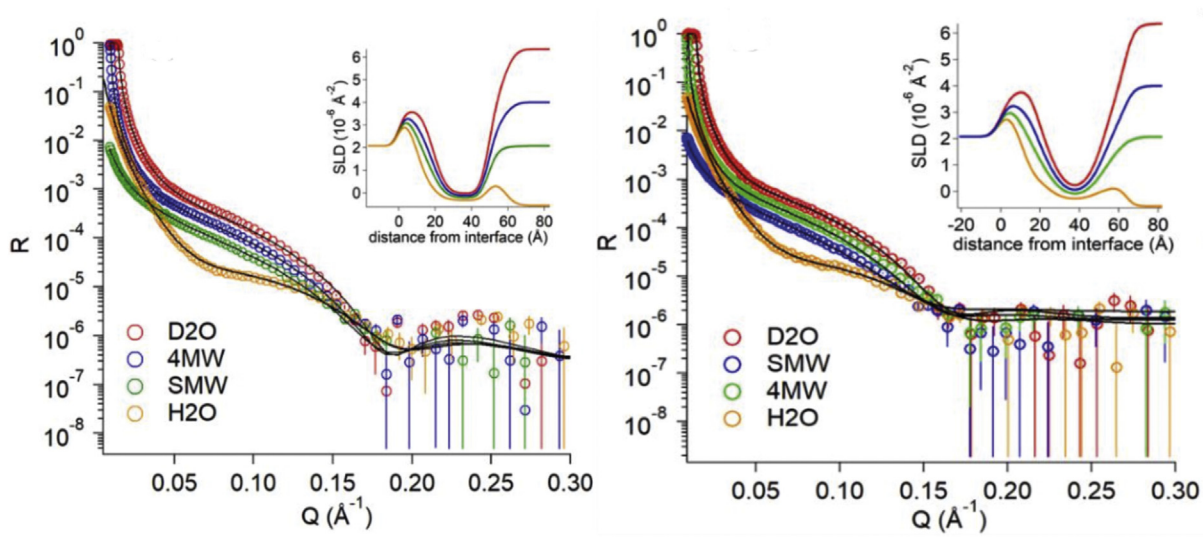

B

Parameter	POPC/Sitosterol	GIPC/POPC/Sitosterol
Bilayer formation	Yes	Yes
% solvent in the tails	5	5
Inner Sugar (Å)	-	4
Inner Head (Å)	8	8
Tail (Å)	31	31
Outer Head (Å)	8	8
Outer Sugar (Å)	-	4

C

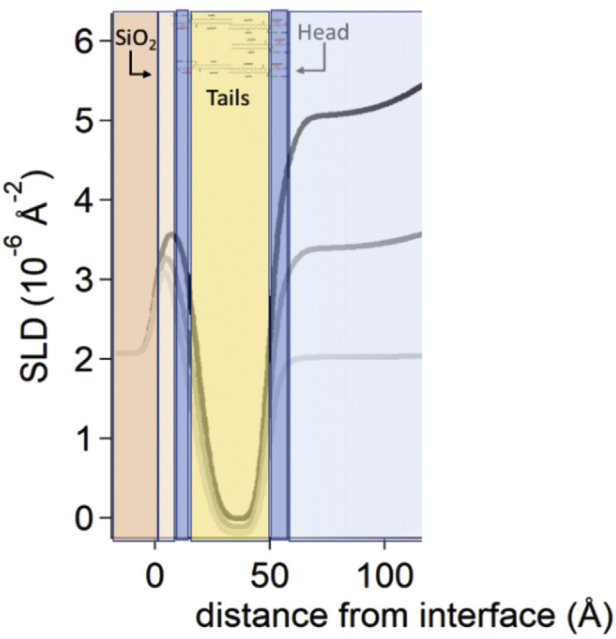

Figure 9. Reflectivity profiles of GIPC-containing lipid bilayer. Reflectivity profiles and calculated scattering length density (SLD) following lipid bilayer deposition of (i) POPC/β-sitosterol (70:30, mol/mol) and (ii) GIPC/POPC/β-sitosterol (55:15:30, mol/mol). *A*, the multilayer model was composed from the silicon substrate (SLD = 2.07 10^{-6} Å^{-2}) covered with a layer of silicon oxide (SLD = 3.47 10^{-6} Å^{-2}); *B*, structural parameters after multilayer model fitting of reflectivity profiles of lipid bilayer; *C*, scheme showing the SLD profile overlaid on the multilayer model as obtained for POPC/GIPC membrane. GIPC, glycosyl inositol phosphoryl ceramide; POPC, 1-palmitoyl-2-oleoyl-*sn*-glycero-3-phosphocholine.

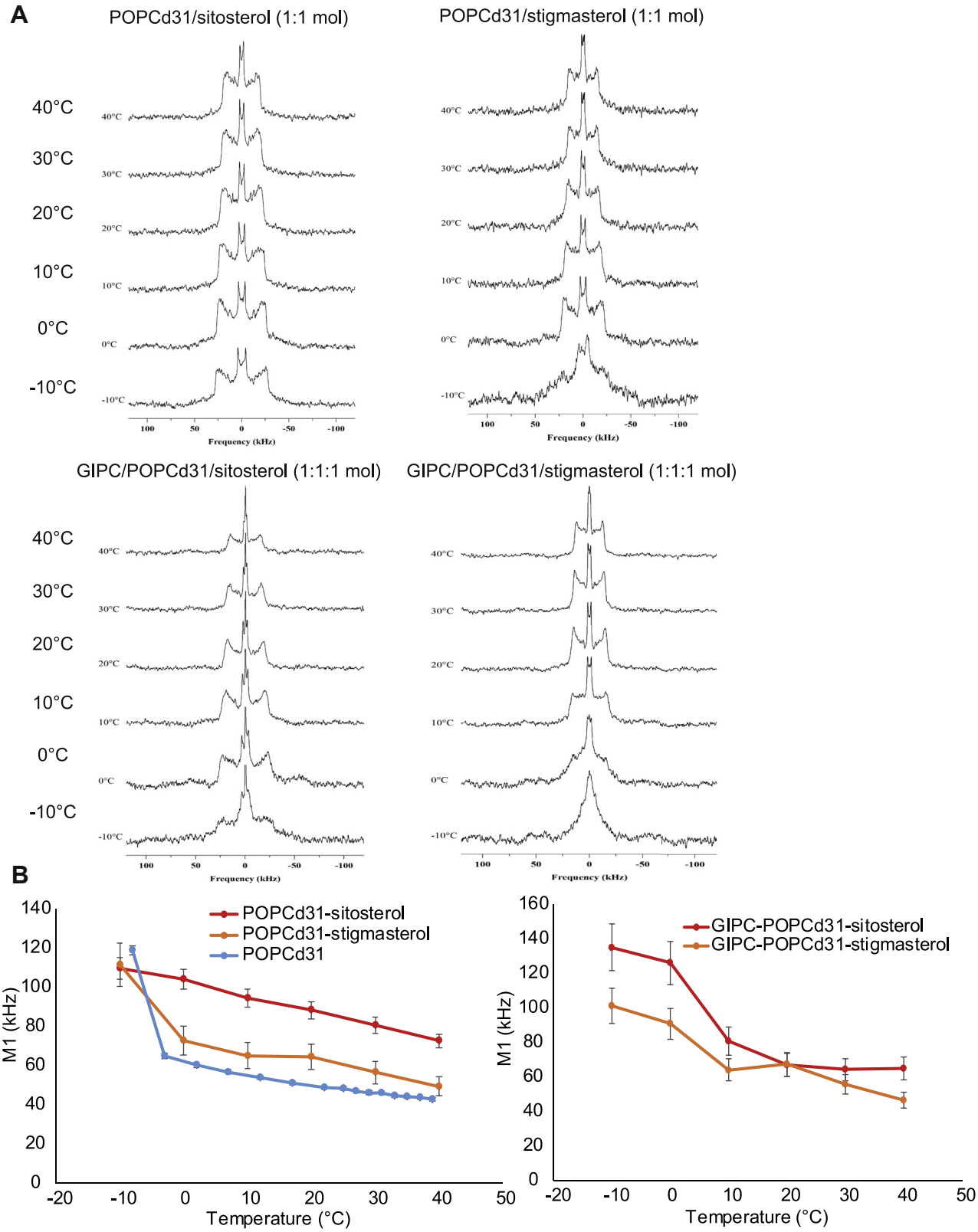

Figure 10. Solid state NMR studies of GIPC-containing liposomes. *A*, ^{2}H-NMR powder spectra of lipid mix, and *B*, first, spectral moment of ^{2}H-NMR spectra showing membrane ordering *versus* temperature POPC-(2)H_{31}system alone, in binary systems of POPC-(2)H_{31}/β-sitosterol (1:1 mol/mol) and POPC-(2)H31/Stigmasterol (1:1 mol/mol) and ternary systems of GIPC/POPC-(2)H31/β-sitosterol (1:1:1 mol ratio) and GIPC/POPC-(2)H31/Stigmasterol (1:1:1 mol ratio). Error bars are mean ± SD from three independent measurements. GIPC, glycosyl inositol phosphoryl ceramide; POPC, 1-palmitoyl-2-oleoyl-*sn*-glycero-3-phosphocholine.

study their biophysical properties. This article describes a protocol for efficient purification of milligram amount of GIPCs. It has been inspired by three publications (11, 12, 35), whereby the steps were rearranged to get rid of contamination such as sterols and glycerolipids during the extraction procedure. This is simpler and more convenient than the one used in previous publications where large amounts of solvents were used. It is also time-efficient and achieve a reasonable yield because we were able to obtain 30 mg of GIPC of up to 85% purity from four distinct plant materials of 600 to 800 g fresh weight. In the near future, to improve yield and purity, we still have to fine-tune the purification and extraction process of GIPCs, and it will also be important to purify different GIPC series individually, so as to decipher the number, bonds, and types of sugar residues which make up the different plant GIPC polar head groups, as was done for fungi GIPC by NMR (53, 54). To do so, ad hoc preparative chromatography needs to be developed with elution solvents with the right polarity.

This study demonstrated that the fractions purified using the newly designed protocol, displayed the signature hVLCFA attributed to sphingolipids with little to no presence of phospholipids (C16 to C18 FA) or sterols (Figs. 2–4). It further established the presence of GIPC with LC-MS experiments, confirming the high purity of our purified GIPC fractions using this particular protocol with no ceramide and glucosylceramide (Data S4). The calculated yield for the different GIPC series was enough to perform all the necessary biophysics experiments for structural analysis and interactant assays.

In all enriched GIPC fractions purified in this study, galacturonic acid and rhamnose are absent (Fig. 4*B*), suggesting no contamination by pectins, particularly Rhamnogalacturonan II, which is reported to bind to GIPCs (37). Previous work in *Arabidopsis thaliana* (*At*, also a Brassicaceae, like cauliflower), identified a Man as the first sugar attached to the GlcA-Ins-P-Cer core in vegetative tissues, a reaction catalyzed by the glycosyltransferase *AtGMT1* (16). We hypothesized that this also might be the case in cauliflower. In the seed tissue of *At*, glucosamine inositol phosphoryl ceramide transferase 1, another glycosyltransferase, adds a GlcNAc instead of a Man to the core structure of GIPC (21). However, in both cases, Ara and Gal were detected as part of the sugar composition of their GIPC enrichments, which might be cell wall contaminant or inherent sugar moieties of GIPC.

The polar head sugar diversity of GIPCs is clearly species-dependent (7). For instance, the increasingly large amounts of Gal and Ara in the Nt-GIPC fractions have been described in (59), where GIPCs of tobacco leaves contain up to four Ara and two Gals attached to the core GIPC structures of GlcN/GlcNAc-GlcA-Ins-P-Cer. Hence, it is correct to assume that the large amount of Ara and Gal of Nt-GIPC(fraction γ) derives from the polyglycosylated GIPCs of up to GIPC series E of Ara-Ara-Gal-Gal-Man-GlcN/GlcNAc-GlcA-Ins-P-Cer.

The full structure and diversity of sugar moieties in the GIPCs polar head remains to be understood and investigated. The diversity seems to be important for example in plant/pathogen interactions. A recent study showed that the GIPC polar head may be receptor for oomycete necrotic toxins called necrosis and ethylene-inducing peptide 1–like (NLPs). Plants enriched in GIPC series A are sensitive to NLPs, whereas those enriched in GIPC series B are insensitive to NLPs, hence conferring resistance against pathogens secreting NLPs (56).

The efficiency of the designed purification protocol as well as the structural differences of sugar moieties listed in the different plant species in this article might expand new possibilities of further studying the complexity of GIPC's intriguing role in membrane organization and in plant immunity. As the most abundant sphingolipid in plants, GIPCs have arguably fundamental roles in molecular and cellular responses that are yet to be discovered. This redesigned protocol allows access to a readily adequate amount of pure GIPCs at the bench from any type of plant tissues.

GIPCs specifically modulate the properties of model membranes

Because GIPCs have large polar heads and VLCFAs, and they tend to agglomerate, we used them in a binary mixture with phospholipids or a ternary mixture with phospholipids and sterols. As expected for lipids with (h)VLCFAs, GIPCs increase the thickness of the model membrane by a few nm, as shown by neutron reflectivity on a supported bilayer (Figs. 8 and 9). The bilayer thickness of liposomes containing GIPCs as observed using cryo-EM are around 6 to 7 nm for the ternary mix, which corresponds well with the observed thickness of purified PM from *Medicago truncatula* and tobacco (57, 58).

One important feature of the PM is its electrostatic charge. PM purification using polymers phase separation PEG/Dextran relies on the fact that PMs are highly negatively charged and that the PM right-side-out fraction is attracted to the positively charged PEG phase (60). The membrane surface charge is regulated by lipids and post transcriptional modification of proteins such as phosphorylation (61). The ζ-potential of GIPC-containing liposomes is −26 mV, five times higher than a PC/β-sitosterol-containing bilayer, likely because of the large negativity of GIPC conferred by its phosphate group and the GlcA residue of the polar head. Therefore, because GIPCs are expected to be mostly located in the outer leaflet of the PM (1), we conclude here that GIPCs contribute strongly to the negative charge of the PM outer leaflet.

GIPCs affect membrane order through specific interactions with different molecular species of phytosterols

Using the biophysical techniques of Langmuir compression isotherms and molecular modeling, we showed that GIPCs interact differentially with different phytosterols. We confirmed that GIPCs with β-sitosterol has a condensation effect as described in (1), whereas noncondensing interactions occur between stigmasterol, SG, or ASG and GIPCs (Figs. 5 and 10). These differential interactions appear to be structure dependent. Just adding a Glc head group (SG) and an acyl chain (ASG) or an unsaturation (C22 in stigmasterol) to the β-sitosterol steryl moieties changes the interaction with the GIPCs and modifies the properties of the model membranes

(Figs. 5–7). Interestingly, GIPCs, ASG, and SG all accumulate after drought stress (62). The differential interaction of GIPCs with the different kind of sterols could explain how plants cope with such stress.

As mentioned, stigmasterol also displayed a non-condensation effect. The structural difference between sitosterol and stigmasterol is only an unsaturation on C22. This has a dramatic effect on membrane fluidity as discussed in (29). Using model membranes and environment-sensitive probes, they showed that plant lipids promote various spatial organization of membrane and that β-sitosterol promotes *Lo* phases while stigmasterol has a low ordering effect and is correlated with low level of *Lo* phases. Plant sterols and sphingolipids form lipid rafts which are signaling platforms (58, 63). These structures can be clearly seen as lipid domains in model monolayers containing β-sitosterol and GIPC that interact with each other (Fig. 7). This interaction might translate into *Lo* phases. Stigmasterol, on the other hand, tends to sequester small structures containing GIPC which might contribute to membrane fluidity.

Potential functions of GIPCs in plant physiology based on these structural information

Plants are poikilothermic and have to adapt the viscosity of their membrane to temperature changes, a process called homeoviscosity. By modulating the fluidity of their membrane to be functionally viable, plants can adapt to temperature fluctuations. For example, plants can readily convert β-sitosterol to stigmasterol by expressing the C22 desaturase CYP710 during temperature acclimation (64). Specific plant membrane components like β-sitosterol, stigmasterol, and glucosylcerebrosides are synthesized as part of temperature adaptations to make membrane-associated biological processes possible (30). Here, we showed that GIPCs are more conducive to enable homeoviscosity. It will be interesting to further investigate how GIPCs are involved in modulating PM fluidity in thermal adaptation in synergy with other PM lipid components.

Recent studies provide new insight on the importance role of GIPC structure in plants through genetic approach (15, 16, 21, 48). By generating mutants combined to the multidisciplinary approaches, we can uncover more about GIPC intricate structure and its biological implications. The modification of the ceramide length and hydroxylation of GIPC might alter the organization of the membrane as does SM in animal cell, which is responsible for interdigitating between the bilayers and domain formation with cholesterol (65, 66). The closest biological molecule in terms of membrane structuring role of plant GIPC series A and B could be SM, even if the latter—absent in plant PM—is made up of a phosphocholine head group. The theoretical model of plant PM showed GIPC as the major sphingolipid in the outer leaflet, just like SM, and inducing a lateral segregation to form *Lo* phases with phytosterols (1, 40). Interestingly, the exact distribution of sterols in the two layers of the PM is still a matter of debate, including in animal biology research fields (67). To know where sitosterol or stigmasterol are located and how they regulate the fluidity of one or both of the PM leaflets are of great interest. Unfortunately, the tools to study phytosterol distribution remain to be developed.

Plant GIPCs are structurally homologous to the animal gangliosides that are absent in plants. Gangliosides are acidic glycolipids containing sialic acid in their polar head that play an important role in immunity, signal transduction in the PM that essential for brain, and retinal functions in animal cells (68, 69). It is possible that polyglycosylated GIPCs have a similar role to gangliosides. Further investigation will require a better understanding of the GIPC glycosylation pattern and the enzymes involved in GIPC biosynthesis. The present study paves the way for tackling the function of plant glycosylated sphingolipids in membrane organization and function.

Experimental procedures

Plant material

Cauliflower and leek were store-bought. Wild-type tobacco (cv. Bright Yellow) cell culture and rice cell culture were obtained as previously described in (8, 19) respectively.

Extraction and purification of GIPCs

The green parts of the cauliflower and leek were removed to prevent contamination by galactolipids, which are mainly present in chloroplasts. Plant material (800 g fresh weight) was blended with 5 l of cold 0.1 N aqueous acetic acid in a chilled stainless-steel Waring Blender at low, medium, and high speed for 30s each. The slurry was filtered through 16 layers of acid-washed Miracloth. The residue was re-extracted once (twice for leek) again in the same manner. The aqueous acetic acid filtrate was discarded. The residue was air-dried overnight under a fume hood and was then refluxed with 2 l of hot 70% ethanol (0.1 N in HCl) for 20 min. The slurry was filtered hot through 16 layers of Miracloth prewashed with acidic ethanol (pressed well to remove all liquid). This process was repeated twice more using a total of 5 l of acidic ethanol. The combined filtrates were chilled at −20 °C for 48 h. The precipitate was removed by centrifugation at 30,000*g* (14,000 rpm at using a Sorvall SLA-1500 rotor) at 4 °C for 15 min. Sphingolipids were then extracted from the precipitates in hot isopropanol/hexane/water (55:20:25, v/v). The solution was homogenized using an Ultra-Turrax for 20 s and incubated at 60 °C for 20 min. After centrifugation at 3000*g* for 10 min, the supernatant was decanted to another tube, and the residue extracted twice more with the hot solvent. A total of 100 ml of solvent was used at this step. The supernatants were combined, and its lipid content was analyzed by TLC and GC-MS to evaluate the amount of GIPC content.

Porous silica beads (Silica gel for chromatography 60 Å, 75–125 μm, Acros Organics), were used throughout for packing the column chromatography. The column consists of 70 ml of silica beads, sand of Fontainebleau, followed by the sphingolipid sample dried in 20 ml of silica beads (see Fig. 2). The column was washed and equilibrated with chloroform. Apolar lipids were washed with a mix of chloroform/methanol of different volume ratios of increasing polarity (4:1 then 3:1

and 2:1). The volume used was equivalent to 4-fold the volume of the column. The column was then eluted with a step gradient of chloroform:methanol:water. Solvent A was chloroform:methanol:water (59:37.5:3.5, v/v) and the solvent B chloroform:methanol:water (46:42:12, v/v). The step gradient elution started with 100% A to end with 100% B, with 10% intervals. The volume of elution corresponds to 2-fold the volume of the column. 1/100th of each elution fractions were collected and dried for GC-MS and TLC analysis to test the purity of the fractions. Fractions containing the same type of GIPCs were pooled and dried. The estimated quantity of GIPC is assessed by calculating the amount of (h)VLCFA. (h)VLCFA represents 1/3 of total GIPC molecular mass.

High-performance thin-layer chromatography analysis

HPTLC plates were Silicagel 60 F254 (Merck). HPTLC plates were impregnated for 3 min with freshly prepared 0.2 M ammonium acetate in methanol, and further dried at 110 °C for 15 min. Purified lipids as well as crude extracts were chromatographed in chloroform/methanol/4N NH_4OH (9:7:2, v/v) on. Lipids were located under UV after staining with Primuline in acetone/water 80/20.

Carbohydrate analysis

Samples (0.2 mg) were hydrolyzed with fresh 2 M TFA at 120 °C for either 1 h, 3 h, or 4 h. The supernatants were retained, dried in a vacuum concentrator, redissolved in 2 ml of water, and filtered through 0.22 μm filters. Samples were analyzed by high-performance anion-exchange chromatography on an ICS-5000 instrument (Thermo Fisher Scientific) equipped with a CarboPac PA20 analytical anion exchange column (3 mm × 150 mm; Thermo Fisher Scientific), a PA20 guard column (3 mm × 30 mm; Thermo Fisher Scientific), a borate trap, and a pulsed amperometric detector. The column was equilibrated with 40 mM NaOH for 5 min before injection of the sample. Monosaccharides were separated using the following methods: a linear gradient from 4 mM NaOH to 3 mM NaOH in the first 6 min, followed by a linear gradient of 3 mM NaOH to 1 mM NaOH from 6 to 8 min. An isocratic gradient was held at 1 mM NaOH from 8 to 23 min and then increased to 450 mM NaOH to elute the acidic sugars from 23.1 min to 45 min. Monosaccharide standards were used for quantification.

Fatty acid analysis

Each sample was transmethylated at 110 °C overnight in methanol containing 5% (v/v) sulfuric acid and spiked with 10 mg of heptadecanoic acid (c17:0) and 10 mg of 2-hydroxytetradecanoic acid (h14:0) as internal standards. After cooling, 3 ml of NaCl (2.5%, w/v) was added, and the released fatty acyl chains were extracted in hexane. Extracts were washed with 3 ml of saline solution (200 mM NaCl and 200 mM Tris, pH 8), dried under a gentle stream of nitrogen and dissolved in 150 ml of N,O-Bis(triméthylsilyl)trifluoroacetamide and trimethylchlorosilane. Free hydroxyl groups were derivatized at 110 °C for 30 min, surplus N,O-Bis(triméthylsilyl) trifluoroacetamide–trimethylchlorosilane was evaporated under nitrogen, and samples were dissolved in hexane for analysis using GC-MS under the same conditions as described (7). Quantification of fatty acids and hydroxyl acids was based on peak areas, which were derived from total ion current, and using the respective internal standards.

Langmuir monolayer trough

Purified GIPC-enriched fractions were used in this study. A solution at 0.4 mM in chloroform:methanol:water (30:60:8) was prepared. Sterols and PLPC were purchased from Avanti Polar Lipids. They were dissolved at 0.4 mM in chloroform:methanol (2:1). The surface pressure-area isotherms were recorded by means of an automated Langmuir trough (KSV Minitrough [width, 75 mm; area, 24.225 mm^2]; KSV Instruments) equipped with a platinum plate attached to a Wilhelmy-type balance. The GIPC sample was heated to 60 °C for 15 min for a better solubilization. Pure solutions and lipid mixtures were spread (fixed volume of 30 μl) as tiny droplets to form a uniform monolayer on a Tris:NaCl 10:150 mM (Millipore) subphase adjusted to pH 7 with HCl. After evaporation of the solvent (15 min), monolayers were compressed at a rate of 5 mm/min and at a temperature of 22 °C ± 1 deg. C. Before each experiment, the cleanliness of the system was confirmed by checking the surface pressure over the surface compression of the pure subphase. At least two independent experiments (distinct sample preparations) with three repetitions for each of them (distinct deposition of the same sample) were performed. The variation coefficient in surface pressure and area was found to be 10% or less.

Molecular modeling approaches

The Hypermatrix docking procedure was used to study the interaction of GIPC with the different sterols, as already described in (1). Briefly, one GIPC molecule is positioned and fixed for the whole calculation at the center of the system, oriented at the hydrophobic/hydrophilic interface. The interacting molecule is also oriented at the hydrophobic/hydrophilic interface, and by rotations and translations, more than 10 million positions of the interacting molecule around the central molecule are calculated. The lowest energy matching is considered as the most stable interaction. Refer to (1) for more details.

Liposomes preparation (freeze and thaw method)

The lipid solution of 1 mg/ml (GIPC/PLPC or POPC or DOPC/Stigmasterol or β-sitosterol) at different molar ratio was dried and resuspended in water. Several cycles of freeze and thaw were done with freezing occurring in liquid nitrogen for 5 min and thawing at 50 °C for 15 min.

LUV preparation for DLS and ζ-potential

LUVs were prepared as described elsewhere, (70) with small modifications. Briefly, the lipid solution (GIPC/DOPC/Sterol) in 3/1 v/v tetrahydrofuran (THF)/H_2O methanol mixture was

transferred into a round-bottom flask, and the organic solvent was removed by evaporation under high vacuum pumping for 5 h, until complete evaporation of the solvent. The lipid film was then hydrated in an appropriate amount of buffer solution and subjected to 3 to 5 freeze thaw cycles, yielding multilamellar vesicles. The resulting suspensions (1 g l^{-1}) were then successively extruded 20 times through 200 and 100 nm polycarbonate membranes using a mini-extruder (Avanti Polar Lipids).

DLS and ζ-potential values

DLS measurements were performed with a Malvern NanoZS instrument operating with a 2 mW HeNe laser at a wavelength of 632.8 nm and detection at an angle of 173°. All measurements were performed in a temperature-controlled chamber at 20 °C (±0.05 °C). Three measurements of 15 runs each were usually averaged. The intensity size distribution was obtained from the analysis of the correlation function using the multiple narrow mode algorithm of the Malvern DTS software. The electrophoretic mobility of the vesicles was measured by using the same Malvern NanoZS apparatus performing at 17° from which the ζ-potential values are determined by applying the Henry equation. The ζ-potential values and the ζ-deviation were averaged over at least three measurements with at least 30 runs per measurement. They were expressed as mean ± SD (n ≥ 3).

GUV preparation (Teflon method)

GUV was prepared as previously described by Kubsch *et al.* (47). Briefly, 50 µl of lipid mixture (1 mg ml^{-1}) dissolved in organic solvent mixture was deposited on a precleaned Teflon disk, and the solvent was evaporated with vacuum for 2 h. The disk was then placed in a 4 ml sealed glass vial with 200 mM sucrose and 50 mM NaCl at 60 °C for 12 h, until a cloudy deposit was formed. For microscopy observation, one volume of the vesicle suspension was mixed with four volumes of iso-osmolar Glc/NaCl solution for better contrast.

Cryogenic electronic microscopy

Lacey carbon formvar 300 mesh copper grids were used. They were first submitted to a standard glow discharged procedure (3 mbar, 3 mA for 40 s). Plunge freezing was realized using the EM-GP apparatus (Leica). Four microliters of the sample was deposited on the grid and immediately blotted for 2 s with a Whatmann paper grade 5 before plunging into a liquid ethane bath cooled with liquid nitrogen (−184 °C). The settings of the chamber were fixed at 70% humidity and 20 °C. Total lipid concentration was 0.3 mg/ml. Lipids molar ratio was as followed: POPC-(2)H_{31}/sterol (2:1), and GIPC/POPC-(2)H_{31}/Sitosterol (1:1:1). Specimens were observed at −170 °C using a cryo holder (626, Gatan), with a ThermoFisher FEI Tecnai F20 electron microscope operating at 200 kV under low-dose conditions. Images were acquired with an Eagle 4k x 4k camera (ThermoFisher FEI) and processed in ImageJ. Deuterated POPC (POPC-(2)H_{31}) were bought from Avanti and used as a marker for NMR measurements, and GIPCs were prepared from cauliflower. Sitosterol and stigmasterol were store bought from Avanti.

Neutron reflectivity

Neutron reflectivity experiments were performed at the ILL, on the FIGARO reflectometer (71), on SLBs formed through vesicle fusion on silicon crystals (72, 73). The crystals (dimensions l × w × h of 80 × 50 × 10 mm^3) were polished through bath sonication in different solvents (5 min in chloroform; 5 min in acetone; 5 min in ethanol) followed by plasma cleaning. The substrates were then extensively rinsed with milliQ water and stored in milliQ water before use.

The specular reflectivity (R) is defined as the ratio of reflected intensity over incident intensity of a neutron beam, when the angle of reflection is equal to the angle of incidence. It is measured from a flat surface using a highly collimated neutron beam as a function of momentum transfer Q, where $Q = 4\pi sin\theta/\lambda$, with θ glancing angle and λ wavelength. The measured reflectivity depends on the variation in the scattering length density profile, ρ(z), perpendicular to the surface. The scattering length density profile over the z-axis was modeled as a sum of discrete contributions from separate layers, each characterized by a defined scattering length density, with a gaussian roughness contribution for each interface and a solvent penetration degree. The MOTOFIT software (74), which runs in the IGOR Pro environment (http://www.wavemetrics.com), was used for the analysis of the NR curves.

A multilayer model was used to analyze the reflectivity profiles of the SLBs, with fixed scattering length density values calculated for each layer: (i) a first layer of a bulk subphase of Si (ρ = 2.07 × 10^{-6} $Å^{-2}$) and a superficial layer of SiO_2 (ρ = 3.41 × 10^{-6} $Å^{-2}$) were introduced. Their thickness and interfacial roughness were characterized in control NR measurements in D_2O and H_2O before vesicle injection. (ii) The polar headgroups of the SLB of the inner and outer leaflet (ρ = 1.86 × 10^{-6} $Å^{-2}$). (iii) The bilayer lipid chains (ρ = −0.30 × 10^{-6} $Å^{-2}$) (75). (iv) The sugar heads of the GIPC were represented as additional layer to the phosphate polar head group in the inner and outer leaflets (ρ = 1.9 × 10^{-6} $Å^{-2}$). (v) Finally, a bulk super phase of solvent was introduced to the model.

All measurements were performed in four contrast solvents, namely H_2O (ρ = −0.56 × 10^{-6} $Å^{-2}$), D_2O (ρ = 6.34 × 10^{-6} $Å^{-2}$), 4 MW (34% H_2O and 66% D_2O, ρ= 4.0 × 10^{-6} $Å^{-2}$), or SMW (62% H_2O and 38% D_2O,ρ= 2.07 × 10^{-6} $Å^{-2}$).

Solid state ^{2}H-NMR

Samples were prepared by co-solubilizing the appropriate amount of Bo-GIPC, POPC (2)H31, sitosterol, and stigmasterol in chloroform. Solvent was evaporated under a flow of nitrogen to obtain a thin lipid film, rehydrated with ultra-pure water before one-night lyophilization. The lipid powder was finally hydrated with 100 µl of deuterium-depleted water

(hydration of 97%). Samples were transferred into 100 µl 4-mm zirconia rotors for NMR analyses. ^{2}H-solid-state nuclear magnetic resonance experiments were performed at 76.77 MHz with a phase-cycled quadrupolar echo pulse sequence (90x-t-90y-t-acq) (76) and using a Bruker Avance III 500 MHz WB (11.75 T) spectrometer equipped with a solid state CPMAS 4 mm H/F/X probe (IECB structural biophysics platform). Acquisition parameters were as follows: spectral window of 500 kHz, π/2 pulse width of 3.5 µs, interpulse delays of 40 µs, recycling delay of 2 s; number of scans from 1K to 6K. Spectra were processed using a Lorentzian line broadening of 300 Hz before Fourier transformation from the top of the echo. Samples were equilibrated for 20 min at a given temperature before data acquisition. All spectra were processed and analyzed using Bruker Topspin 4.0.6 software. First moments were calculated using a C^{2+} homemade routine (S. Buchoux, unpublished results).

LC-MS analysis

For the analysis of sphingolipids by LC-MS/MS, lipids extracts were then incubated 1 h at 50 °C in 2 ml of methylamine solution (7 ml methylamine 33% (w/v) in EtOH combined with 3 ml of methylamine 40% (w/v) in water (Sigma Aldrich) to remove phospholipids. After incubation, methylamine solutions dried at 40 °C under a stream of air (35). Finally, were resuspended into 100 µl of THF/MeOH/H2O (40:20:40, v/v) with 0.1% formic acid containing synthetic internal lipid standards (Cer d18:1/C17:0, GluCer d18:1/C12:0 and monosialotetrahexosylganglioside) was added, thoroughly vortexed, incubated at 60 °C for 20 min, sonicated 2 min, and transferred into LC vials. LC-MS/MS (multiple reaction monitoring mode) analyses were performed with a model QTRAP 6500 (ABSciex) mass spectrometer coupled to a liquid chromatography system (1290 Infinity II, Agilent). Analyses were performed in the positive mode. Nitrogen was used for the curtain gas (set to 30), gas 1 (set to 30), and gas 2 (set to 10). Needle voltage was at +5500 V with needle heating at 400 °C; the declustering potential was adjusted between +10 and +40 V. The collision gas was also nitrogen; collision energy varied from +15 to +60 eV on a compound-dependent basis. Reverse-phase separations were performed at 40 °C on a Supercolsil ABZ+, 100 × 2.1 mm column and 5 µm particles (Supelco). The Eluent A was THF/ACN/5 mM Ammonium formate (3/2/5 v/v/v) with 0.1% formic acid and eluent B was THF/ACN/5 mM Ammonium formate (7/2/1 v/v/v) with 0.1% formic acid. The gradient elution program for Cer and GluCer quantification was as follows: 0 to 1 min, 1% eluent B; 40 min, 80% eluent B; and 40 to 42, 80% eluent B. The gradient elution program for GIPC quantification was as follows: 0 to 1 min, 15% eluent B; 31 min, 45% eluent B; 47.5 min, 70% eluent B; and 47.5 to 49, 70% eluent B. The flow rate was set at 0.2 ml/min, and 5 ml sample volumes were injected. The areas of LC peaks were determined using MultiQuant software (version 3.0; ABSciex) for sphingolipids quantification, see Table S1 the list of molecules Q1 ions and Q3 ions.

Data availability

All data contained within the manuscript in form of main figures, table, and supplementary materials.

Supporting information—This article contains supporting information.

Acknowledgments—M. D. and L. L. thank the FRS-FNRS for their position as Senior Research Associates. They benefited from the facilities and expertise of the Biophysical and Structural Chemistry platform (BPCS) at IECB, CNRS UMS3033, INSERM US001, Bordeaux University http://www.iecb.ubordeaux.fr/index.php/fr/plateformestechnologiques. We thank the Bordeaux Metabolomics and Lipidomics Platform (https://www.biomemb.cnrs.fr/en/). We thank Jean-Paul Douliez, Catherine Sarazin and Sébastien Buchoux for critical reading and advice and Laure Beven for bright field microscopy. We thank Claire Bréhélin for the help in electronic microscopy observations. We thank Yuri Gerelli for the neutron analysis.

Author contributions—A. M. C. designed and performed GIPC purification; A. M. C. and A. G. performed and analyzed data of NMR; M. D. and O. L. performed and analyzed data of cryoEM; L. F. and D. B. performed and analyzed data of LC-MS; Y. N., L. H., and G. F. performed neutron experiments and liposomes measurements; A. M. C. with contributions of L. F. and P. V. D. performed lipid analysis; Y. G. and J. C. M. performed and analyzed GIPC sugar content; M. D. and A. M. C. performed and analyzed Langmuir experiments; L. L. did the calculations for molecular modeling; L. M. -P. contributed to additional research funding for A. M. C. PhD project; M. N. contributed to rice culture cells; A. M. C., M. D., L. L., F. S. -P., and S. M. wrote the paper, and all authors carefully revised it.

Funding and additional information—A. M. C. PhD project was funded by the French Ministry of Higher Education and Research (MESR). F. S. -P., S. M., L. L., L. F., and D. B. are funded by the ANR PlayMobil (ANR-19-CE20-0016-02). Y. G., J. C. M. were funded as was part of the DOE Joint BioEnergy Institute (http://www.jbei.org) supported by the U. S. Department of Energy, Office of Science, Office of Biological and Environmental Research, through contract DE-AC02-05CH11231 between Lawrence Berkeley National Laboratory and the U. S. Department of Energy. We thank Bordeaux-Metabolome platform for lipid analysis supported by ANR PlayMobil (grant no. ANR-19-CE20-0016-02 to S. M., L. F., F. S. -P.) and Bordeaux Metabolome Facility-MetaboHUB (grant no. ANR-11-INBS-0010 to S. M. and L. F.).

Conflict of interest—The authors declare no conflict of interest.

Abbreviations—The abbreviations used are: ΔGex, excess free energy of the mixing; ΔGM, the free energy of mixing; Ap-GIPC, *Allium porrum* (leek) GIPC; Ara, arabinose; ASG, acyl steryl glucoside; Bo-GIPC, *Brassica oleracea* (cauliflower) GIPC; C22, fatty acid with 22 carbon atoms; cryo-EM, cryo electronic microscopy; DLS, dynamic light scattering; DOPC, 1,2-dioleoyl-sn-glycero-3-phosphocholine; FA, fatty acid chain; Gal, galactose; GalA, galacturonic acid; GC-MS, Gas chromatography coupled to mass spectrometry; GIPC, glycosyl inositol phosphoryl ceramide; Glc, glucose; GlcA, glucuronic acid; GlcN, glucosamine; GlcNAc,

N-acetyl-glucosamine; GluCer, Glucosyl ceramide; GUV, giant unilamellar vesicle; HPTLC, High-performance thin-layer chromatography; hVLCFA, 2-hydroxylated VLCFA; IPC, inositol phosphoryl ceramide; LCB, long chain base; Lo, liquid-ordered; LUV, large unilamellar vesicles; Man, mannose; NLP, necrosis and ethylene-inducing peptide 1–like; Nt-GIPC, *Nicotiana tabacum* (tobacco) BY-2 GIPC; Os-GIPC, *Oryza sativa* (rice) GIPC; PC, phosphatidylcholine; PLPC, 1-Palmitoyl-2-linoleoyl-sn-glycero-3-phosphocholine; PM, plasma membrane; POPC, 1-palmitoyl-2-oleoyl-sn-glycero-3-phosphocholine; SG, steryl glucoside; SLB, supported lipid bilayers; SM, sphingomyelin; THF, tetrahydrofuran; VLCFA, Very-long chain fatty acid; Xyl, xylose.

References

1. Cacas, J. L., Buré, C., Grosjean, K., Gerbeau-Pissot, P., Lherminier, J., Rombouts, Y., Maes, E., Bossard, C., Gronnier, J., Furt, F., Fouillen, L., Germain, V., Bayer, E., Cluzet, S., Robert, F., *et al.* (2016) Revisiting plant plasma membrane lipids in tobacco: A focus on sphingolipids. *Plant Physiol.* **170**, 367–384
2. Yetukuri, L., Ekroos, K., Vidal-Puig, A., and Orešič, M. (2008) Informatics and computational strategies for the study of lipids. *Mol. Biosyst.* **4**, 121–127
3. Markham, J. E., Lynch, D. V., Napier, J. A., Dunn, T. M., and Cahoon, E. B. (2013) Plant sphingolipids: Function follows form. *Curr. Opin. Plant Biol.* **16**, 350–357
4. Hannun, Y. A., and Obeid, L. M. (2018) Sphingolipids and their metabolism in physiology and disease. *Nat. Rev. Mol. Cell Biol.* **19**, 175–191
5. Carter, H. E., Gigg, R. H., Law, J. H., Nakayama, T., and Weber, E. (1958) Biochemistry of the sphingolipides. XI. Structure of phytoglycolipide. *J. Biol. Chem.* **233**, 1309–1314
6. Pata, M. O., Hannun, Y. A., and Ng, C. K. Y. (2010) Plant sphingolipids: Decoding the enigma of the sphinx. *New Phytol.* **185**, 611–630
7. Buré, C., Cacas, J. L., Wang, F., Gaudin, K., Domergue, F., Mongrand, S., and Schmitter, J. M. (2011) Fast screening of highly glycosylated plant sphingolipids by tandem mass spectrometry. *Rapid Commun. Mass Spectrom.* **25**, 3131–3145
8. Cacas, J. L., Buré, C., Furt, F., Maalouf, J. P., Badoc, A., Cluzet, S., Schmitter, J. M., Antajan, E., and Mongrand, S. (2013) Biochemical survey of the polar head of plant glycosylinositolphosphoceramides unravels broad diversity. *Phytochemistry* **96**, 191–200
9. Hsieh, T. C., Lester, R. L., and Laine, R. A. (1981) Glycophosphoceramides from plants. Purification and characterization of a novel tetrasaccharide derived from tobacco leaf glycolipids. *J. Biol. Chem.* **256**, 7747–7755
10. Carter, H. E., and Kisic, A. (1969) Countercurrent distribution of inosol lipids of plant seeds. *J. Lipid Res.* **10**, 356–362
11. Carter, H. E., and Koob, J. L. (1969) Sphingolipids in bean leaves (Phaseolus vulgaris). *J. Lipid Res.* **10**, 363–369
12. Kaul, K., and Lester, R. L. (1975) Characterization of inositol-containing phosphosphingolipids from tobacco leaves. *Plant Physiol.* **55**, 120–129
13. Sperling, P., and Heinz, E. (2003) Plant sphingolipids: Structural diversity, biosynthesis, first genes and functions. *Biochim. Biophys. Acta* **1632**, 1–15
14. Buré, C., Cacas, J. L., Badoc, A., Mongrand, S., and Schmitter, J. M. (2016) Branched glycosylated inositolphosphosphingolipid structures in plants revealed by MS3 analysis. *J. Mass Spectrom.* **51**, 305–308
15. Mortimer, J. C., Yu, X., Albrecht, S., Sicilia, F., Huichalaf, M., Ampuero, D., Michaelson, L. V., Murphy, A. M., Matsunaga, T., Kurz, S., Stephens, E., Baldwin, T. C., Ishii, T., Napier, J. A., Weber, A. P., *et al.* (2013) Abnormal glycosphingolipid mannosylation triggers salicylic acid-mediated responses in Arabidopsis. *Plant Cell* **25**, 1881–1894
16. Fang, L., Ishikawa, T., Rennie, E. A., Murawska, G. M., Lao, J., Yan, J., Tsai, A. Y., Baidoo, E. E., Xu, J., Keasling, J. D., Demura, T., Kawai-Yamada, M., Scheller, H. V., and Mortimer, J. C. (2016) Loss of inositol phosphorylceramide sphingolipid mannosylation induces plant immune responses and reduces cellulose content in arabidopsis. *Plant Cell* **28**, 2991–3004
17. Luttgeharm, K. D., Kimberlin, A. N., Cahoon, R. E., Cerny, R. L., Napier, J. A., Markham, J. E., and Cahoon, E. B. (2015) Sphingolipid metabolism is strikingly different between pollen and leaf in Arabidopsis as revealed by compositional and gene expression profiling. *Phytochemistry* **115**, 121–129
18. Tellier, F., Maia-Grondard, A., Schmitz-Afonso, I., and Faure, J. D. (2014) Comparative plant sphingolipidomic reveals specific lipids in seeds and oil. *Phytochemistry* **103**, 50–58
19. Nagano, M., Ishikawa, T., Fujiwara, M., Fukao, Y., Kawano, Y., Kawai-Yamada, M., and Shimamoto, K. (2016) Plasma membrane microdomains are essential for Rac1-RbohB/H-mediated immunity in rice. *Plant Cell* **28**, 1966–1983
20. Rennie, E. A., Ebert, B., Miles, G. P., Cahoon, R. E., Christiansen, K. M., Stonebloom, S., Khatab, H., Twell, D., Petzold, C. J., Adams, P. D., Dupree, P., Heazlewood, J. L., Cahoon, E. B., and Scheller, H. V. (2014) Identification of a sphingolipid α-glucuronosyltransferase that is essential for pollen function in Arabidopsis. *Plant Cell* **26**, 3314–3325
21. Ishikawa, T., Fang, L., Rennie, E. A., Sechet, J., Yan, J., Jing, B., Moore, W., Cahoon, E. B., Scheller, H. V., Kawai-Yamada, M., and Mortimer, J. C. (2018) GLUCOSAMINE INOSITOLPHOSPHORYLCERAMID-TRANSFERASE1 (GINT1) is a GlcNAc-containing glycosylinositol phosphorylceramide glycosyltransferase. *Plant Physiol.* **177**, 938–952
22. Mortimer, J. C., and Scheller, H. V. (2020) Synthesis and function of complex sphingolipid glycosylation. *Trends Plant Sci.* **25**, 522–524
23. Kaiser, H. J., Lingwood, D., Levental, I., Sampaio, J. L., Kalvodova, L., Rajendran, L., and Simons, K. (2009) Order of lipid phases in model and plasma membranes. *Proc. Natl. Acad. Sci. U. S. A.* **106**, 16645–16650
24. Levental, I., and Veatch, S. L. (2016) The continuing mystery of lipid rafts. *J. Mol. Biol.* **428**, 4749–4764
25. Lingwood, D., and Simons, K. (2010) Lipid rafts as a membrane-organizing principle. *Science* **327**, 46–50
26. Baumgart, T., Hunt, G., Farkas, E. R., Webb, W. W., and Feigenson, G. W. (2007) Fluorescence probe partitioning between Lo/Ld phases in lipid membranes. *Biochim. Biophys. Acta* **1768**, 2182–2194
27. Mannock, D. A., Lewis, R. N. A. H., McMullen, T. P. W., and McElhaney, R. N. (2010) The effect of variations in phospholipid and sterol structure on the nature of lipid-sterol interactions in lipid bilayer model membranes. *Chem. Phys. Lipids* **163**, 403–448
28. Gerbeau-Pissot, P., Der, C., Thomas, D., Anca, I. A., Grosjean, K., Roche, Y., Perrier-Cornet, J. M., Mongrand, S., and Simon-Plas, F. (2014) Modification of plasma membrane organization in tobacco cells elicited by cryptogein. *Plant Physiol.* **164**, 273–286
29. Grosjean, K., Mongrand, S., Beney, L., Simon-Plas, F., and Gerbeau-Pissot, P. (2015) Differential effect of plant lipids on membrane organization specificities of phytosphingolipids and phytosterols. *J. Biol. Chem.* **290**, 5810–5825
30. Beck, J. G., Mathieu, D., Loudet, C., Buchoux, S., and Dufourc, E. J. (2007) Plant sterols in "rafts": A better way to regulate membrane thermal shocks. *FASEB J.* **21**, 1714–1723
31. Furt, F., Lefebvre, B., Cullimore, J., Bessoule, J. J., and Mongrand, S. (2007) Plant lipid rafts: Fluctuat nec mergitur. *Plant Signal. Behav.* **2**, 508–511
32. Moreau, R. A., Nyström, L., Whitaker, B. D., Winkler-Moser, J. K., Baer, D. J., Gebauer, S. K., and Hicks, K. B. (2018) Phytosterols and their derivatives: Structural diversity, distribution, metabolism, analysis, and health-promoting uses. *Prog. Lipid Res.* **70**, 35–61
33. Sonnino, S., and Prinetti, A. (2010) Gangliosides as regulators of cell membrane organization and functions. *Adv. Exp. Med. Biol.* **688**, 165–184
34. Lingwood, D., Binnington, B., Róg, T., Vattulainen, I., Grzybek, M., Coskun, Ü., Lingwood, C. A., and Simons, K. (2011) Cholesterol modulates glycolipid conformation and receptor activity. *Nat. Chem. Biol.* **7**, 260–262
35. Markham, J. E., and Jaworski, J. G. (2007) Rapid measurement of sphingolipids from Arabidopsis thaliana by reversed-phase high-performance liquid chromatography coupled to electrospray ionization tandem mass spectrometry. *Rapid Commun. Mass Spectrom.* **21**, 1304–1314
36. Mamode Cassim, A., Gouguet, P., Gronnier, J., Laurent, N., Germain, V., Grison, M., Boutté, Y., Gerbeau-Pissot, P., Simon-Plas, F., and

Mongrand, S. (2019) Plant lipids: Key players of plasma membrane organization and function. *Prog. Lipid Res.* **73**, 1–27
37. Voxeur, A., and Fry, S. C. (2014) Glycosylinositol phosphorylceramides from Rosa cell cultures are boron-bridged in the plasma membrane and form complexes with rhamnogalacturonan II. *Plant J.* **79**, 139–149
38. Kitazawa, K., Tryfona, T., Yoshimi, Y., Hayashi, Y., Kawauchi, S., Antonov, L., Tanaka, H., Takahashi, T., Kaneko, S., Dupree, P., Tsumuraya, Y., and Kotake, T. (2013) β-galactosyl yariv reagent binds to the β-1,3-galactan of arabinogalactan proteins. *Plant Physiol.* **161**, 1117–1126
39. Deleu, M., Crowet, J. M., Nasir, M. N., and Lins, L. (2014) Complementary biophysical tools to investigate lipid specificity in the interaction between bioactive molecules and the plasma membrane: A review. *Biochim. Biophys. Acta* **1838**, 3171–3190
40. Tjellström, H., Hellgren, L. I., Wieslander, Å., and Sandelius, A. S. (2010) Lipid asymmetry in plant plasma membranes: Phosphate deficiency-induced phospholipid replacement is restricted to the cytosolic leaflet. *FASEB J.* **24**, 1128–1138
41. Maget-Dana, R. (1999) The monolayer technique: A potent tool for studying the interfacial properties of antimicrobial and membrane-lytic peptides and their interactions with lipid membranes. *Biochim. Biophys. Acta* **1462**, 109–140
42. Marsh, D. (1996) Lateral pressure in membranes. *Biochim. Biophys. Acta* **1286**, 183–223
43. Róg, T., and Pasenkiewicz-Gierula, M. (2004) Non-polar interactions between cholesterol and phospholipids: A molecular dynamics simulation study. *Biophys. Chem.* **107**, 151–164
44. Smondyrev, A. M., and Berkowitz, M. L. (2001) Molecular dynamics simulation of the structure of dimyristoylphosphatidylcholine bilayers with cholesterol, ergosterol, and lanosterol. *Biophys. J.* **80**, 1649–1658
45. Yeagle, P. L., Martin, R. B., Lala, A. K., Lin, H. K., and Bloch, K. (1977) Differential effects of cholesterol and lanosterol on artificial membranes. *Proc. Natl. Acad. Sci. U. S. A.* **74**, 4924–4926
46. Róg, T., Pasenkiewicz-Gierula, M., Vattulainen, I., and Karttunen, M. (2009) Ordering effects of cholesterol and its analogues. *Biochim. Biophys. Acta* **1788**, 97–121
47. Kubsch, B., Robinson, T., Steinkühler, J., and Dimova, R. (2017) Phase behavior of charged vesicles under symmetric and asymmetric solution conditions monitored with fluorescence microscopy. *J. Vis. Exp.* https://doi.org/10.3791/56034
48. Jiang, Z., Zhou, X., Tao, M., Yuan, F., Liu, L., Wu, F., Wu, X., Xiang, Y., Niu, Y., Liu, F., Li, C., Ye, R., Byeon, B., Xue, Y., Zhao, H., *et al.* (2019) Plant cell-surface GIPC sphingolipids sense salt to trigger Ca2+ influx. *Nature* **572**, 341–346
49. Seelig, J. (1977) Deuterium magnetic resonance: Theory and application to lipid membranes. *Q. Rev. Biophys.* **10**, 353–418
50. Davis, J. H. (1983) The description of membrane lipid conformation, order and dynamics by 2H-NMR. *Biochim. Biophys. Acta* **737**, 117–171
51. Kang, S. Y., Gutowsky, H. S., and Oldfield, E. (1979) Spectroscopic studies of specifically deuterium labeled membrane systems. Nuclear magnetic resonance investigation of protein-lipid interactions in Escherichia coli membranes. *Biochemistry* **18**, 3268–3272
52. Seneviratne, V., Frech, R., and Furneaux, J. E. (2003) Phases and phase transitions of P(EO)6LiSbF6. *Electrochim. Acta* **48**, 2221–2226
53. Simenel, C., Coddeville, B., Delepierre, M., Latgé, J. P., and Fontaine, T. (2008) Glycosylinositolphosphoceramides in Aspergillus fumigatus. *Glycobiology* **18**, 84–96
54. Gutierrez, A. L. S., Farage, L., Melo, M. N., Mohana-Borges, R. S., Guerardel, Y., Coddeville, B., Coddeville, B., Wieruszeski, J. M., Mendonça-Previato, L., and Previato, J. O. (2007) Characterization of glycoinositolphosphoryl ceramide structure mutant strains of Cryptococcus neoformans. *Glycobiology* **17**, 1C–11C
55. Buré, C., Cacas, J. L., Mongrand, S., and Schmitter, J. M. (2014) Characterization of glycosyl inositol phosphoryl ceramides from plants and fungi by mass spectrometry. *Anal. Bioanal. Chem.* **406**, 995–1010
56. Lenarčič, T., Albert, I., Böhm, H., Hodnik, V., Pirc, K., Zavec, A. B., Podobnik, M., Pahovnik, D., Žagar, E., Pruitt, R., Greimel, P., Yamaji-Hasegawa, A., Kobayashi, T., Zienkiewicz, A., Gömann, J., *et al.* (2017) Eudicot plant-specific sphingolipids determine host selectivity of microbial NLP cytolysins. *Science* **358**, 1431–1434
57. Lefebvre, B., Furt, F., Hartmann, M. A., Michaelson, L. V., Carde, J. P., Sargueil-Boiron, F., Rossignol, M., Napier, J. A., Cullimore, J., Bessoule, J. J., and Mongrand, S. (2007) Characterization of lipid rafts from Medicago truncatula root plasma membranes: A proteomic study reveals the presence of a raft-associated redox system. *Plant Physiol.* **144**, 402–418
58. Mongrand, S., Morel, J., Laroche, J., Claverol, S., Carde, J. P., Hartmann, M. A., Bonneu, M., Simon-Plas, F., Lessire, R., and Bessoule, J. J. (2004) Lipid rafts in higher plant cells: Purification and characterization of triton X-100-insoluble microdomains from tobacco plasma membrane. *J. Biol. Chem.* **279**, 36277–36286
59. Kaul, K., and Lester, R. L. (1978) Isolation of six novel phosphoinositol-containing sphingolipids from tobacco leaves. *Biochemistry* **17**, 3569–3575
60. Morré, D. M., and Morre, D. J. (2000) Aqueous two-phase partition applied to the isolation of plasma membranes and Golgi apparatus from cultured mammalian cells. *J. Chromatogr. B Biomed. Sci. Appl.* **743**, 377–387
61. Goldenberg, N. M., and Steinberg, B. E. (2010) Surface charge: A key determinant of protein localization and function. *Cancer Res.* **70**, 1277–1280
62. Tarazona, P., Feussner, K., and Feussner, I. (2015) An enhanced plant lipidomics method based on multiplexed liquid chromatography-mass spectrometry reveals additional insights into cold- and drought-induced membrane remodeling. *Plant J.* **84**, 621–633
63. Gronnier, J., Gerbeau-Pissot, P., Germain, V., Mongrand, S., and Simon-Plas, F. (2018) Divide and rule: Plant plasma membrane organization. *Trends Plant Sci.* **23**, 899–917
64. Morikawa, T., Mizutani, M., Aoki, N., Watanabe, B., Saga, H., Saito, S., Oikawa, A., Suzuki, H., Sakurai, N., Shibata, D., Wadano, A., Sakata, K., and Ohta, D. (2006) Cytochrome P450 CYP710A encodes the sterol C-22 desaturase in Arabidopsis and tomato. *Plant Cell* **18**, 1008–1022
65. Róg, T., Orłowski, A., Llorente, A., Skotland, T., Sylvänne, T., Kauhanen, D., Ekroos, K., Sandvig, K., and Vattulainen, I. (2016) Interdigitation of long-chain sphingomyelin induces coupling of membrane leaflets in a cholesterol dependent manner. *Biochim. Biophys. Acta* **1858**, 281–288
66. London, E., and Brown, D. A. (2000) Insolubility of lipids in Triton X-100: Physical origin and relationship to sphingolipid/cholesterol membrane domains (rafts). *Biochim. Biophys. Acta* **1508**, 182–195
67. Courtney, K. C., Fung, K. Y. Y., Maxfield, F. R., Fairn, G. D., and Zha, X. (2018) Comment on 'orthogonal lipid sensors identify transbilayer asymmetry of plasma membrane cholesterol'. *Elife* **7**, 1–8
68. Sipione, S., Monyror, J., Galleguillos, D., Steinberg, N., and Kadam, V. (2020) Gangliosides in the brain: Physiology, pathophysiology and therapeutic applications. *Front. Neurosci* **14**, 572965
69. Sibille, E., Berdeaux, O., Martine, L., Bron, A. M., Creuzot-Garcher, C. P., He, Z., Thuret, G., Bretillon, L., and Masson, E. A. (2016) Ganglioside profiling of the human retina: Comparison with other ocular structures, brain and plasma reveals tissue specificities. *PLoS One* **11**, e0168794
70. Navon, Y., Radavidson, H., Putaux, J. L., Jean, B., and Heux, L. (2017) PH-sensitive interactions between cellulose nanocrystals and DOPC liposomes. *Biomacromolecules* **18**, 2918–2927
71. Campbell, R. A., Wacklin, H. P., Sutton, I., Cubitt, R., and Fragneto, G. (2011) Figaro: The new horizontal neutron reflectometer at the ILL. *Eur. Phys. J. Plus* **126**, 1–22
72. Montis, C., Gerelli, Y., Fragneto, G., Nylander, T., Baglioni, P., and Berti, D. (2016) Nucleolipid bilayers: A quartz crystal microbalance and neutron reflectometry study. *Colloids Surf. B Biointerfaces* **137**, 203–213
73. Richter, R. P., Bérat, R., and Brisson, A. R. (2006) Formation of solid-supported lipid bilayers: An integrated view. *Langmuir* **22**, 3497–3505
74. Nelson, A. (2006) Co-refinement of multiple-contrast neutron/X-ray reflectivity data using MOTOFIT. *J. Appl. Crystallogr.* **39**, 273–276
75. Wacklin, H. P. (2010) Neutron reflection from supported lipid membranes. *Curr. Opin. Colloid Interf. Sci.* **15**, 445–454
76. Davis, J. H., Jeffrey, K. R., Bloom, M., and Valic, M. (1976) Quadrupolar echo deuteron magnetic resonance spectroscopy in ordered hydrocarbon chains. *Chem. Phys. Lett.* **42**, 390–394
77. Eeman, M., Deleu, M., Paquot, M., Thonart, P., and Dufrêne, Y. F. (2005) Nanoscale properties of mixed fengycin/ceramide monolayers explored using atomic force microscopy. *Langmuir* **21**, 2505–2511